Atmos. Chem. Phys., 13, 12363–12388, 2013
www.atmos-chem-phys.net/13/12363/2013/
doi:10.5194/acp-13-12363-2013

Atmospheric Chemistry and Physics Open Access

Climatology of pure tropospheric profiles and column contents of ozone and carbon monoxide using MOZAIC in the mid-northern latitudes (24° N to 50° N) from 1994 to 2009

R. M. Zbinden[1,*], V. Thouret[1], P. Ricaud[2], F. Carminati[1,2], J.-P. Cammas[1,], and P. Nédélec[1]**

[1]Laboratoire d'Aérologie, UMR5560, CNRS and Université de Toulouse, Toulouse, France
[2]CNRM-GAME, UMR3589, Météo-France et CNRS, Toulouse, France
[*]now at: CNRM-GAME, UMR3589, Météo-France et CNRS, Toulouse, France
[**]now at: OSUR, UMS3365, Université de la Réunion, Saint-Denis, La Réunion, France

Correspondence to: R. M. Zbinden (regina.zbinden@meteo.fr)

Received: 7 May 2013 – Published in Atmos. Chem. Phys. Discuss.: 5 June 2013
Revised: 28 October 2013 – Accepted: 7 November 2013 – Published: 18 December 2013

Abstract. The objective of this paper is to deliver the most accurate ozone (O_3) and carbon monoxide (CO) climatology for the pure troposphere only, i.e. exclusively from the ground to the dynamical tropopause on an individual profile basis. The results (profiles and columns) are derived solely from the **M**easurements of **OZ**one and water vapour by in-service **AI**rbus air**C**raft programme (MOZAIC) over 15 years (1994–2009). The study, focused on the northern mid-latitudes [24–50° N] and [119° W–140° E], includes more than 40 000 profiles over 11 sites to give a quasi-global zonal picture. Considering all the sites, the pure tropospheric column peak-to-peak seasonal cycle ranges are 23.7–43.2 DU for O_3 and 1.7–6.9 $\times 10^{18}$ molecules cm^{-2} for CO. The maxima of the seasonal cycles are not in phase, occurring in February–April for CO and May–July for O_3. The phase shift is related to the photochemistry and OH removal efficiencies. The purely tropospheric seasonal profiles are characterized by a typical autumn–winter/spring–summer O_3 dichotomy (except in Los Angeles, Eastmed – a cluster of Cairo and Tel Aviv – and the regions impacted by the summer monsoon) and a summer–autumn/winter–spring CO dichotomy. We revisit the boundary-layer, mid-tropospheric (MT) and upper-tropospheric (UT) partial columns using a new monthly varying MT ceiling. Interestingly, the seasonal cycle maximum of the UT partial columns is shifted from summer to spring for O_3 and to very early spring for CO. Conversely, the MT maximum is shifted from spring to summer and is associated with a summer (winter) MT thickening (thinning). Lastly, the pure tropospheric seasonal cycles derived from our analysis are consistent with the cycles derived from spaceborne measurements, the correlation coefficients being $r = 0.6$–0.9 for O_3 and $r > 0.9$ for CO. The cycles observed from space are nevertheless greater than MOZAIC for O_3 (by 9–18 DU) and smaller for CO (up to 1×10^{18} molecules cm^{-2}). The larger winter O_3 difference between the two data sets suggests probable stratospheric contamination in satellite data due to the tropopause position. The study underlines the importance of rigorously discriminating between the stratospheric and tropospheric reservoirs and avoiding use of a monthly averaged tropopause position without this strict discrimination in order to assess the pure O_3 and CO tropospheric trends.

1 Introduction

Tropospheric ozone (O_3) is a key parameter for both air quality and climate issues. In the boundary layer (BL), O_3 is harmful to humans (West et al., 2007), animals and vegetation (Felzer et al., 2007). In the upper troposphere, O_3 impacts on radiative forcing (Forster and Shine, 1997; Aghedo et al., 2011; Riese et al., 2012). O_3 also controls the oxidizing capacity of the atmosphere. The tropospheric ozone distribution results from complex in situ photochemical production and interactions with dynamical processes such as stratospheric export (Junge, 1962; Danielsen, 1968; Wernli and Bourqui, 2002; Stohl et al., 2003), free tropospheric

subsidence (Guttikunda et al., 2005) or boundary-layer venting (Agusti-Panareda et al., 2005; Auvray et al., 2005) and long-range transport (Cooper et al., 2010). In addition to O_3, carbon monoxide (CO) is also involved in tropospheric photochemical processes: O_3 production takes place when CO and hydrocarbons are photo-oxidized in the presence of nitrogen oxides (NO_x). CO is a by-product of combustion from the BL and an excellent tropospheric air-mass tracer due to its rather long lifetime of ~ 2 months on average (Yurganov et al., 2004).

Tropospheric O_3 distribution analysis started in the 1960s with soundings that were sparse in space and time (3–12 per month) over about 40 northern hemispheric sites (Logan, 1985, 1994, 1999). Fishman and Larsen (1990) later began tropospheric O_3 retrieval by remote sensing satellites and performed climatology analysis. From satellites, the O_3 / CO correlations were investigated recently to provide the strength of O_3 photochemical production and to show the continental outflow regions in the middle free troposphere (Zhang et al., 2006; Voulgarakis et al., 2011). Nevertheless, satellite observations still cannot replace in situ measurements because of their need for permanent calibration, their time dependence, low vertical resolution, cloud screening, etc. Since August 1994, the MOZAIC (Measurements of OZone and water vapour by in-service AIrbus airCraft; Marenco et al., 1998) instruments on board commercial aircraft have sampled the troposphere with high vertical resolution over about 50 airports and IAGOS (In-service Aircraft for Global Observing System) is the current ongoing programme (see the MOZAIC/IAGOS website[1]).

The purpose and novelty of the present study is to produce, from the MOZAIC measurements, the first pure tropospheric climatology of O_3 and CO based on fully defined individual tropospheric profiles. The new methodology aims to improve the previous MOZAIC O_3 tropospheric climatology presented by Zbinden et al. (2006), which was restricted by the permanent 12 km limit of MOZAIC aircraft during ascent or descent. Here, all profiles are defined individually from the surface to the dynamical tropopause and include all sampled stratospheric intrusions. Furthermore, the study, based on such new profiles and their associated columns, encompasses a larger range of longitudes from Los Angeles to Japan in the northern mid-latitudes [24–50° N].

The paper first briefly describes the MOZAIC data (Sect. 2) and explains the methodology (Sect. 3). The climatological results are presented in Sect. 4 for the monthly averaged tropospheric columns, the seasonally averaged tropospheric profiles and the boundary-layer, mid- and upper-tropospheric partial tropospheric columns. To further highlight the usefulness of such a climatology, we compare the O_3 and CO tropospheric seasonal cycles from our analysis with those derived from spaceborne measurements at two MOZAIC sites in Europe and Asia. Section 5 concludes our analysis.

[1] http://www.iagos.fr/ or via http://www.pole-ether.fr

2 MOZAIC data

The MOZAIC programme has collected numerous O_3 observations since 1994 by using instruments on board five commercial aircraft (Marenco et al., 1998) throughout the troposphere and lower stratosphere. The O_3 is measured using the dual-beam UV absorption principle (Model 49–103 from Thermo Environmental Instruments, USA), with an accuracy estimated at $\pm[2\,\text{ppbv} + 2\,\%]$ and a 4 s time response, i.e. < 50 m vertical resolution (Thouret et al., 1998). Measurement quality control procedures have remained unchanged to ensure that long-term series are free of instrumental artefacts since the beginning of the programme. Instruments are laboratory calibrated before and after a flight period of about 6–12 months. The infrared CO analyser (Model 48CTL from Thermo Environmental Instruments, USA) included in the MOZAIC programme since 2001 measured CO with a ± 5 ppbv ($\pm 5\,\%$) accuracy for a 30 s response time (< 300 m vertical resolution) (Nédélec et al., 2003).

To characterize the vertical distribution over the troposphere, we selected the ascents and descents from the 4 s full-resolution data between August 1994 and March 2009. The results, focused on the northern mid-latitudes [24–50° N] and on longitudes from Los Angeles to Japan [119° W–140° E], are based on 11 sites among those most regularly visited by the MOZAIC aircraft (see details in Table 1). To improve the sampling frequency of a few sites and to avoid wide data gaps in the time series, we have created clusters including data from neighbouring airports with the same seasonal cycles and monthly mean concentrations. For example, Germany is the cluster of Frankfurt and Munich, the most visited site (16 041 profiles). Selecting only Frankfurt would have left data gaps of two months in 2002 and six months in 2005. By adding Munich airport, which is close (500 km) to Frankfurt even though at higher surface altitude (500 m), we obtain continuous time series relevant for climatological studies. Japan is the cluster of Tokyo, Nagoya and Osaka airports on the south-eastern coast (≤ 500 km distance). Houston and Dallas airports form the USsouth cluster (250 km distance). In total, $> 40\,000$ profiles are compiled here (Table 1), i.e. more than twice the number of the profiles used in a previous study (Zbinden et al., 2006).

3 Methodology

Our objective is to deliver a monthly mean pure tropospheric climatology of profiles and columns for O_3 and CO based on the ascent or descent phase of MOZAIC flights, strictly from the surface to the altitude of the dynamical tropopause z_{DT} as defined by Hoskins et al. (1985) (Thouret et al., 2006; Zbinden et al., 2006). The dynamical tropopause criterion

Table 1. Geographical context of the study over four continents (column 1) with the MOZAIC site labelling (column 2), the related airport or airports for a cluster (column 3), the airport geographic coordinates (column 4), the number of associated MOZAIC profiles (Nb P, column 5), the airport elevation (column 6) and total number of MOZAIC profiles included in this study (bottom line).

Continent	Site label	Airport or cluster	Geographic coordinates	Nb P	Elevation (m a.s.l.)
	Los Angeles	Los Angeles	[118.17° W, 34.00° N]	300	38
North	USeast	Washington, New York, Boston	[77.00° W, 38.92° N], [73.63° W, 40.67° N], [71.00° W, 42.50° N]	5054	5, 4, 6
America	USlake	Chicago, Detroit, Toronto	[87.60° W, 41.75° N], [83.34° W, 42.21° N], [79.00° W, 43.00° N]	2425	204, 196, 173
	USsouth	Dallas, Houston	[96.80° W, 32.80° N], [95.25° W, 29.45° N]	2315	185, 30
	Paris	Paris	[2.58° E, 49.00° N]	4379	119
Europe	Germany	Frankfurt, Munich	[9.00° E, 50.00° N], [11.78° E, 48.34° N]	16 041	111, 453
	Vienna	Vienna	[16.37° E, 48.20° N]	4765	183
Middle	Eastmed	Cairo, Tel Aviv	[31.39° E, 30.10° N], [34.89° E, 32.00° N]	702	116, 41
East	Uaemi	Abu Dhabi, Dubai	[54.64° E, 24.44° N], [55.35° E, 25.26° N]	953	27, 19
Asia	Beijing	Beijing	[111.50° E, 40.00° N]	906	35
	Japan	Osaka, Nagoya, Tokyo	[135.00° E, 34.00° N], [136.80° E, 35.10° N], [139.70° E, 35.60° N]	3098	11, 14, 43
			Total Nb of profiles	40 938	

is more adapted than the lapse rate to capturing the tropospheric ozone trends (on sites where statistics are significant) and to distinguish the contribution of the stratospheric exchanges from the strict troposphere in further studies. Additionally, the dynamical tropopause has been already used in satellite/in situ comparison (Clerbaux et al., 2008; Hegglin et al. 2008; de Laat et al., 2009; Bak et al., 2013). Furthermore, some technical reasons reinforce the choice of using a dynamical tropopause instead of the lapse rate criterion as explained in Sect. 3.1. However, the troposphere may not be completely sampled by MOZAIC aircraft during individual ascent or descent due to a permanent ≈ 12 km limitation. The tropospheric layer frequently unvisited by MOZAIC was ignored or partially estimated in the previous study by Zbinden et al. (2006). For example, over Germany, the thickness of the tropospheric layer unvisited by MOZAIC is 0.8 km on average but might exceed 3.8 km over Japan in August. In this section, the methodology for deriving the pure tropospheric profiles and columns is explained, followed by the ozonesonde validation of these new products.

3.1 Pure tropospheric results assessment

At a specific site, a MOZAIC profile, $\mathrm{MP}(X,z,t)$, is defined for a molecule X, such as O_3 and CO at a given time, t, between z_0 and z_{top}, i.e. the surface altitude and the highest altitude of the ascent or descent phase of the flight, with a 50 m resolution in z. The pure tropospheric profile, $\mathrm{PTP}(X,z,t)$, should simply result from the $\mathrm{MP}(X,z,t)$ without the stratospheric air above z_{DT} at time t. To deliver consistent results between profiles, columns and satellite results, the O_3 volume mixing ratio at a given altitude z and time t is converted into a partial column of 50 m height resolution, expressed in Dobson units (DU) (see Zbinden et al., 2006, Appendix A) using its related measured temperature and pressure. Similarly, the CO volume mixing ratio is converted into molecules cm^{-2}. To set up z_{DT} at time t, the potential vorticity pressure of 2 PVU is used, referring to the study by Thouret et al. (2006) with MOZAIC data when selecting only the cruise part of flights to document the upper troposphere–lower stratosphere. The potential vorticity pressures provided by the operational European Centre for Medium-Range Weather Forecast (ECMWF) analyses (T213) are interpolated for the specific aircraft positions and available with a 150 m vertical resolution on the MOZAIC database (Thouret et al., 2006; Zbinden et al., 2006).

The methodology to assess the pure tropospheric profiles, explained just below, is illustrated in Fig. 1 with three typical cases selected over Germany ((a) 8 December 1994, (b) 10 May 2000) and Japan ((c) 16 August 1995). When $z_{\mathrm{DT}} < z_{\mathrm{top}}$, and only in this case, MOZAIC samples the entire troposphere (Fig. 1a). In all other cases, a tropospheric layer remains undefined between z_{top} and z_{DT}, Δ, as shown in Fig. 1b and c. If the lapse rate criterion (WMO, 1957) was selected instead of a dynamical criterion, the thermal tropopause could have been fixed only at an altitude (z_{lr}) below z_{top}-1 km. The different z_{top}, z_{s} and z_{DT} are shown in Fig. 1 and additionally z_{lr} in Fig. 1a. Consequently, using z_{lr} instead of z_{DT}, more profiles would be turned into uncompleted tropospheric profiles without any perspective to be completed. The particular MOZAIC vertical sampling leads to $\mathrm{TP}(X,z,t)$, the tropospheric profiles up to z_{DT} or at least z_{top} at time t, from which a preliminary climatology is calculated on a seasonal (s) basis, $\overline{\mathrm{TP}}(X,z,s)$.

In Zbinden et al. (2006), we estimated Δ at time t, using $\overline{\mathrm{TP}}(X,z,s)$ above z_{top}. Nevertheless, $\overline{\mathrm{TP}}(X,z,s)$ is still strictly limited to z_{s}, the ascent- or descent-phase maximum altitude within the season s, and is always less than 12 km. Consequently, Δ is fully evaluated only when $z_{\mathrm{DT}} < z_{\mathrm{s}}$, hereafter noted Δ_{s} (Fig. 1b).

In this study, at time t, when $z_{\mathrm{DT}} > z_{\mathrm{s}}$ (Fig. 1c), we additionally evaluated Δ_f between z_{s} and z_{DT} by using $\mathrm{Mfit}(X, z_{\Delta_f}, s)$, the best-fit line from MOZAIC data using a linear regression on $\overline{\mathrm{TP}}(X,z,s)$, from 5 to 11 km for O_3 and from 8 to 11 km for CO. These limits in altitude were chosen to be as far as possible from the polluted BL but not

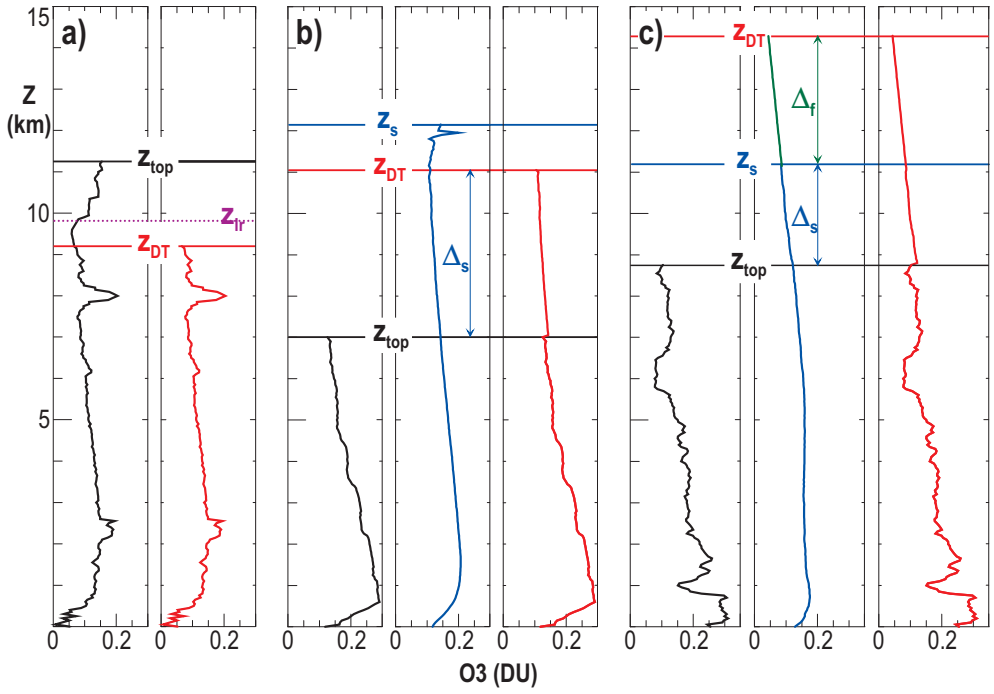

Fig. 1. Pure tropospheric profiles up to z_{DT}, PTP(O_3, z, t) (red), from three typical individual MOZAIC profiles, MP(O_3, z, t) (black), using the preliminary seasonal tropospheric profile, $\overline{\text{TP}}(O_3, z, s)$ (blue). For **(a)** $z_{DT} < z_{top}$, **(b)** $z_{top} < z_{DT} < z_s$ and **(c)** $z_{DT} > z_s$. Δ_s and Δ_f are the layer filled using $\overline{\text{TP}}(O_3, z, s)$ (blue) and Mfit_s (green), respectively. See the text for the definition of z_{DT}, z_{lr}, z_s and z_{top}, the horizontal lines in red, purple, blue and black, respectively.

too high to maintain significant sampling and, by the end, to be representative of the seasonal tropospheric amounts in the upper-tropospheric layers. For CO, similarly, the limits were fixed at higher altitudes but within a narrow layer because CO does not decrease linearly with altitude except above 7–8 km.

Our PTP(X, z, t) derivation can be summarized by the following three typical cases, where $z = [z_0, z_{DT}]$ at time t,

$$\text{PTP}(X, z, t) = \text{MP}(X, z, t) = \text{TP}(X, z, t), \quad (1)$$

$$\text{PTP}(X, z, t) = \text{TP}(X, z^\star, t) + \overline{\text{TP}}(X, z_{\Delta_s}, s), \quad (2)$$

$$\text{PTP}(X, z, t) = \text{TP}(X, z^\star, t) + \overline{\text{TP}}(X, z_{\Delta_s}, s) + \text{Mfit}(X, z_{\Delta_f}, s), \quad (3)$$

and using the equation

(1) – if $z_{DT} < z_{top}$, in case (a), Fig. 1a;

(2) – if $z_{top} < z_{DT} < z_s$, in case (b), Fig. 1b with $z^\star = [z_0, z_{top}]$ and $z_{\Delta_s} = [z_{top}, z_{DT}]$;

(3) – if $z_{top} < z_s < z_{DT}$, in case (c), Fig. 1c with $z^\star = [z_0, z_{top}]$, $z_{\Delta_s} = [z_{top}, z_s]$ and $z_{\Delta_f} = [z_s, z_{DT}]$.

Table 2. Percentage of MP profiles for the three cases where $z_{DT} < z_{top}$, $z_{top} < z_{DT} < z_s$, $z_{top} < z_s < z_{DT}$.

Sites	Percentage of MP with		
	$z_{DT} < z_{top}$	$z_{top} < z_{DT} < z_s$	$z_{top} < z_s < z_{DT}$
Los Angeles	24.3	31.3	44.3
USeast	41.9	31.9	26.2
USlake	43.5	34.3	22.1
USsouth	10.5	26.6	62.8
Paris	46.0	46.0	8.0
Germany	49.5	44.4	6.1
Vienna	58.4	36.3	5.3
Eastmed	34.8	16.3	48.9
Uaemi	4.5	5.1	90.4
Beijing	48.2	36.0	15.8
Japan	31.4	29.3	39.2

Table 2 provides the percentage of profiles corresponding to the 3 cases encountered at the 11 sites. We found more than 50 % of the profiles of Uaemi and USsouth belong to case (c), while less than 8 % for Europe. Note that the database encompasses domestic flights which connect two close airports, such as Abu Dhabi and Dubai (∼ 150 km apart) or Dallas and Houston (∼ 400 km apart). Consequently, cruise level is never reached and the flight is limited to a short ascent and short descent. MOZAIC data over Los Angeles, Eastmed,

Beijing and Vienna do not include domestic flights, while they represent less than 1 % for Germany, USeast, USlake, Japan and Paris, 29 % of the MOZAIC traffic for USsouth, and 39 % for Uaemi, which partly explains Table 2. We did not discarded these profiles because they were documenting the highly variable BL and areas where no regular ozonesondes or carbon monoxide measurements exist.

From $\mathrm{PTC}(X,t)$, we calculated the monthly times series (not shown) and finally the monthly averaged $\mathrm{PTC_m}(X,t)$ as shown in Sect. 4.1. The $\overline{z_{\mathrm{DT}}}$ by month or season is not introduced in any of the $\mathrm{PTC_m}(X,t)$ or $\mathrm{PTP_s}(X,z,t)$ calculations; it is only provided in the figures as a guideline. Consequently, the delivered climatology results from profile and column tropospheric contents on an individual z_{DT} basis, the cornerstone of this study.

Figure 2a shows an example of the monthly averaged MOZAIC O_3 profiles, $\overline{\mathrm{MP}}(\mathrm{O_3},z,m)$, and the monthly averaged pure tropospheric profiles, $\overline{\mathrm{PTP}}(\mathrm{O_3},z,m)$, over Japan for September to November and February, when the monthly averaged z_{DT} varies from 9.4 to 13.4 km. This example highlights that the profiles $\overline{\mathrm{MP}}(\mathrm{O_3},z,m)$ and $\overline{\mathrm{PTP}}(\mathrm{O_3},z,m)$ are identical until an altitude, z_{Ld}, where they deeply diverge, located below the monthly averaged z_{DT}. They show, from the surface to 1 km, a permanent strong positive vertical gradient and, above 1 km and up to z_{Ld}, a sustainable negative vertical gradient. Above z_{Ld}, $\overline{\mathrm{MP}}(\mathrm{O_3},z,m)$ returns to a positive vertical gradient as opposed to $\overline{\mathrm{PTP}}(\mathrm{O_3},z,m)$. Thus, z_{Ld} illustrates the impact of depth penetration of the tropopause and stratospheric air contamination on a monthly basis; this altitude will be used later in Sect. 4.3.1.

Furthermore, the integral along the vertical of $\mathrm{PTP}(X,z,t)$ at time t provides a pure tropospheric column, $\mathrm{PTC}(X,t)$ for a molecule X, such as O_3 and CO, expressed in DU and in molecules cm^{-2}, respectively, with

$$\mathrm{PTC}(X,t)=\sum_{z=z_0}^{z_{\mathrm{DT}}}\mathrm{PTP}(X,z,t). \quad (4)$$

Moreover, the pure tropospheric columns can be decomposed into three partial columns over the boundary-layer (BLC), mid-troposphere (MTC) and upper troposphere columns (UTC). In this study, we have replaced the constant ceiling altitude of MTC (8 km as in Zbinden et al., 2006) by a variable altitude, z_{Ld}, defined as the lowest altitude where $\overline{\mathrm{MP}}(\mathrm{O_3},z,m)$ diverges from $\overline{\mathrm{PTP}}(\mathrm{O_3},z,m)$. An example of the z_{Ld} location over Japan shows variations from 6.0 km in February to 9.0 km in October (Fig. 2a). Thus the partial columns $\mathrm{BLC}(X,t)$, $\mathrm{MTC}(X,t)$ and $\mathrm{UTC}(X,t)$ are integrated over 0–2 km, 2 km $-z_{\mathrm{Ld}}$ and $z_{\mathrm{Ld}}-z_{\mathrm{DT}}$, respectively.

The climatologies are given by month (m) for columns (Sect. 4.1), by season (s) for profiles (Sect. 4.2) and by month for the three partial columns considering the new monthly varying z_{Ld} (Sect. 4.3).

3.2 Pure Tropospheric O_3 validation

This subsection aims to validate the use of $\mathrm{Mfit}(X,z_{\Delta_f},s)$ and ultimately our $\mathrm{PTP}(\mathrm{O_3},z,t)$ and $\mathrm{PTC}(\mathrm{O_3},t)$, with composite profiles combining $\mathrm{TP}(\mathrm{O_3},z,t)$ from MOZAIC and an external in situ data set. The latter data came from the World Ozone and Ultraviolet Radiation Data Centre ozonesondes network (WOUDC hereafter) available for neighbouring areas: Wallops Island for USeast (936 sondes from 22 August 1994 to 27 March 2009 with 640 MOZAIC coincident profiles) Hohenpeissenberg for Germany (1823 sondes from 1 August 1994 to 30 March 2009 with 5127 MOZAIC coincident profiles) and Tateno for Japan (798 sondes from 10 August 1994 to 26 March 2009 with 402 MOZAIC coincident profiles). The effective height resolution of the vertical profile of an ozonesonde is 100–150 m, and the bias, the precision and the accuracy differ with ozonesonde types: electrochemical concentration cell (ECC sondes, Wallops Island), Brewer–Mast (BM sondes, Hohenpeissenberg) and carbon iodine (KC sondes, Tateno), as discussed in details by Smit and Team ASOPOS (2013). They indicate, between the surface and 15 km, that the bias varies from 0 to −7%, the precision from 3 to 10 % and the accuracy from 4 to 13 %. Thus, ozonesonde quality results depend on instrument type, launch conditions and altitude, while MOZAIC does not.

The data processing of WOUDC and MOZAIC is identical. However, to sample similar meteorological situations and improve accuracy, we selected only coincident profiles on both data sets (i.e. within a 24 h interval, denoted t'). Consequently, the sampling frequency is reduced. The coincident results by month are denoted m'. Also, we assumed that z_{DT} at time t' was valid for both coincident data sets. Figure 2b shows the monthly averaged MOZAIC profiles, $\overline{\mathrm{MP}}(\mathrm{O_3},z,m')$, and WOUDC profiles, $\overline{\mathrm{WP}}(\mathrm{O_3},z,m')$, over Japan for the four months as provided in Fig. 2a. The best agreement between these monthly averaged profiles is found when z_{DT} is greater than 12 km on a monthly average. This is an important result because the troposphere is not fully sampled with MOZAIC in such high z_{DT} cases. After discarding the stratospheric air above z_{DT} at time t', the monthly averaged pure tropospheric profiles were derived from MOZAIC and WOUDC as $\overline{\mathrm{MPTP}}(\mathrm{O_3},z,m')$ and $\overline{\mathrm{WPTP}}(\mathrm{O_3},z,m')$, respectively (Fig. 2c). Note that the grey-shaded rectangles of Fig. 2c highlight the layer unvisited by MOZAIC within the month and period and thus the greatest impact of Mfit on the monthly averaged profile climatology. Despite z_{DT} uncertainties and/or co-location errors at time t', it is interesting to note that, as in Zbinden et al. (2006), both coincident tropospheric climatologies exhibit the same, almost straight, negative O_3 vertical gradient above 3 km (also clearly observed in summer over USeast but not shown).

Then, to validate the estimation of Δ on the full MOZAIC data set, we derived a composite profile called MOZAIC-WOUDC pure tropospheric profiles, $\mathrm{MWPTP}(\mathrm{O_3},z,t)$, by adding $\overline{\mathrm{WPTP}}(\mathrm{O_3},z_\Delta,m')$ to $\mathrm{TP}(\mathrm{O_3},z^\star,t)$ over Δ with $z=$

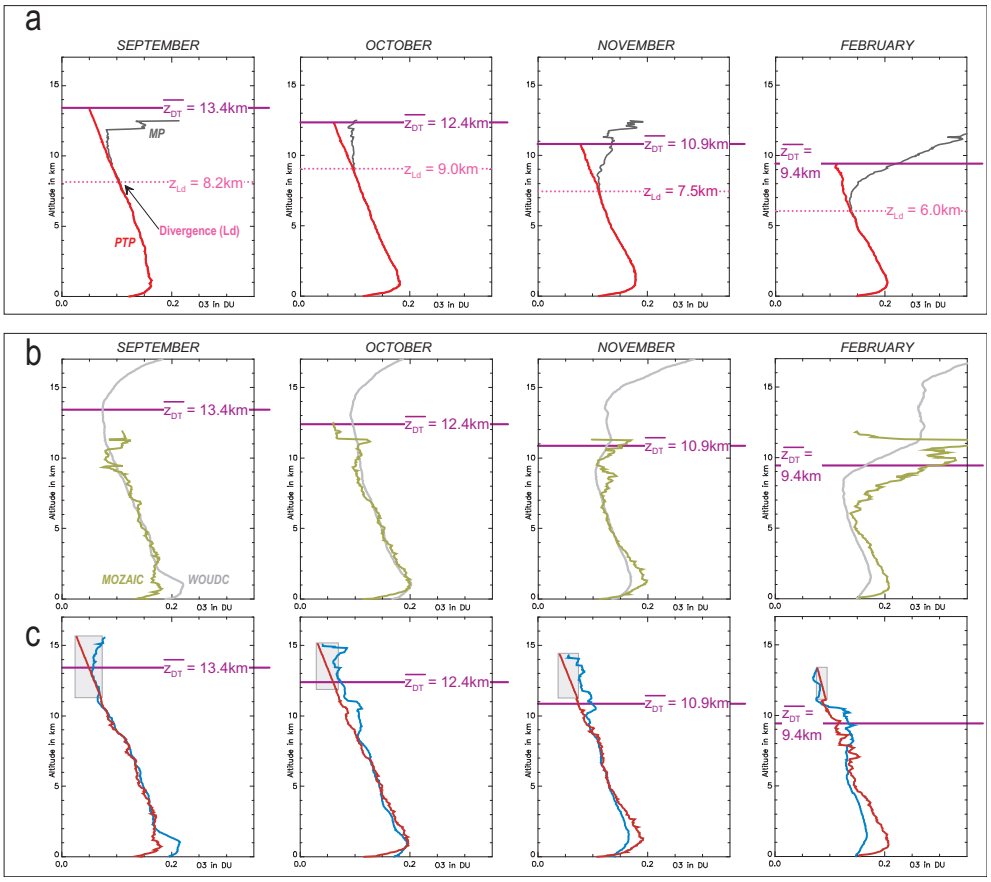

Fig. 2. Methodology **(a)** and validation **(b, c)** illustrated with data sets of MOZAIC over Japan and WOUDC sondes at Tateno (1994–2006) focusing on September, October, November and February profiles (left to right) with various $\overline{z_{DT}}$ (purple horizontal line) on a monthly averaged basis. **(a)**, using the full MOZAIC data set $\overline{MP}(O_3, z, m)$ with $z = [z_0, z_{top}]$ (black) and $\overline{PTP}(O_3, z, m)$ with $z = [z_0, z_{DT}]$ (red). The altitude where $\overline{MP}(O_3, z, m)$ diverges from $\overline{PTP}(O_3, z, m)$ is defined as z_{Ld}, the dotted pink line. **(b)**, using coincident data sets $\overline{MP}(O_3, z, m')$ (green – MOZAIC) and $\overline{WP}(O_3, z, m')$ (grey – WOUDC). **(c)**, using only tropospheric data sets between z_0 and z_{DT} of the coincident data sets $\overline{MPTP}(O_3, z, m')$ (red – MOZAIC) and $\overline{WPTP}(O_3, z, m')$ (blue – WOUDC). The impact of the $Mfit_s$ filling is highlighted in the panels by grey-shaded rectangles. The horizontal axis is O_3 expressed in DU and the vertical axis is altitude in kilometres.

$[z_0, z_{DT}]$, $z^\star = [z_0, z_{top}]$ and $z_\Delta = [z_{top}, z_{DT}]$. Only two cases needed to be considered:

$$MWPTP(O_3, z, t) = TP(O_3, z, t) = PTP(O_3, z, t), \quad (5)$$

$$MWPTP(O_3, z, t) = TP(O_3, z^\star, t) + \overline{WPTP}(O_3, z_\Delta, m'), \quad (6)$$

and Eq. (5) is used when $z_{DT} < z_{top}$, while Eq. (6) is used when $z_{DT} > z_{top}$.

Before providing such a composite result, we checked the consistency of the MOZAIC and WOUDC coincident data sets between 2 and 8 km, $\overline{MPTP}(O_3, z, m')$ and $\overline{WPTP}(O_3, z, m')$. We selected the three most documented and distant sites (USeast, Germany, Japan). The altitude limitation was necessary to avoid the highly variable BL and to take into account the layers with the best MOZAIC sampling rate below z_{DT}. We found that the correlation coefficient is $r > 0.9$ (Fig. 3) at all the sites. Moreover, when integrating the two MOZAIC and WOUDC data sets, the differences were −0.01 DU (−7 %), −0.003 DU (−2 %) and 0.008 DU (0.9 %) on average for USeast, Germany and Japan, respectively. Over Germany the high and regular sampling frequency of both data sets and the small z_{DT} variability contributes to the best quality of results. Furthermore, a WOUDC O_3 excess occurred over USeast regardless of month, over Japan during May–September, and over Germany during all months except March (Table 3). The German range is 0–1 DU or 0–5 % and extreme values are −3.1 DU (14 %) in August over USeast and 1.7 DU (9 %) in February over Japan. Therefore, we consider that our Δ estimate can now be validated by comparing the $\overline{PTP}(O_3, z, m)$ with the composite result $\overline{MWPTP}(O_3, z, m)$.

Finally, using all MOZAIC data sets, we validated the methodology by checking the consistency of $\overline{TC}(O_3, m)$, $\overline{PTC}(O_3, m)$ and $\overline{MWPTC}(O_3, m)$ which are the vertical integration of $\overline{TP}(O_3, z, m)$, $\overline{PTP}(O_3, z, m)$ and $\overline{MWPTP}(O_3, z, m)$, respectively. Figure 4 shows their

Table 3. Difference by month between the integrated content derived from $\overline{\text{MPTP}}(O_3, z, m')$ and $\overline{\text{WPTP}}(O_3, z, m')$ with $z = [2, 8\,\text{km}]$, in coincidence, for USeast, Germany and Japan clusters with the correlation coefficient r (column 2). The differences $\overline{\text{MPTP}}(O_3, z, m') - \overline{\text{WPTP}}(O_3, z, m')$ are given in columns 4–15. The last two columns are the average and standard deviation. In each cell, the difference is expressed in percent and in DU on the first and second line, respectively.

Cluster	r	unit	Jan	Feb	Mar	Apr	May	Jun	Jul	Aug	Sep	Oct	Nov	Dec	Avg.	sd
USeast	0.949	%	−9.87	−7.88	−1.28	−4.74	−8.19	−6.45	−9.42	−14.17	−8.26	−11.02	−2.81	−8.96	−7.75	3.54
		DU	−1.79	−1.44	−0.25	−1.06	−1.94	−1.46	−2.20	−3.13	−1.62	−2.02	−0.47	−1.48	−1.57	0.77
Germany	0.984	%	−1.51	−0.89	0.85	−0.17	−1.40	−1.43	−2.71	−2.09	−4.87	−2.98	−3.03	−2.66	−1.91	1.50
		DU	−0.24	−0.15	0.16	−0.04	−0.30	−0.31	−0.59	−0.44	−0.91	−0.49	−0.48	−0.41	−0.35	0.28
Japan	0.914	%	8.34	9.69	6.33	1.50	−2.70	−4.82	−10.18	−4.51	−1.35	1.51	3.99	3.98	0.98	5.91
		DU	1.31	1.67	1.22	0.32	−0.61	−1.20	−2.10	−0.80	−0.24	0.26	0.64	0.64	0.09	1.12

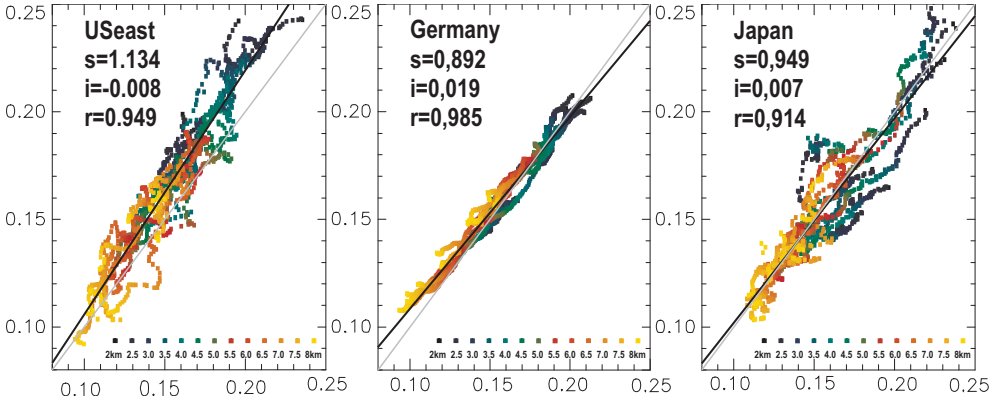

Fig. 3. Comparison of MOZAIC $\overline{\text{MPTP}}(O_3, z, m')$ and WOUDC $\overline{\text{WPTP}}(O_3, z, m')$, with z between 2 and 8 km in coincidence, over USeast (left), Germany (middle) and Japan (right). Measurement altitudes refer to the colour scale, from black (2 km) to yellow (8 km). The slope (s), the intercept (i) and the correlation coefficient (r) of the linear fit (black line) are given for each site with the bisector (grey line). All values are in DU.

seasonal cycles for USeast, Germany and Japan with, in addition and as a guideline, the visualization of the MOZAIC unvisited tropospheric layer Δ. Δ is located between the altitude given by the solid green line, the monthly average of z_{DT} in all cases, and by the dotted green line, the monthly average of z_{DT} if $z_{\text{DT}} < z_{\text{top}}$ and z_{top} if $z_{\text{DT}} > z_{\text{top}}$. The three sites clearly show the same $\overline{\text{PTC}}(O_3, m)$ and $\overline{\text{MWPTC}}(O_3, m)$ seasonal cycles. The bias between $\overline{\text{MWPTC}}(O_3, m)$ and $\overline{\text{PTC}}(O_3, m)$ is less than 2 DU (6 %). Therefore, as the $\overline{\text{PTC}}(O_3, m)$ and $\overline{\text{MWPTC}}(O_3, m)$ correlation coefficient is $r > 0.96$, we conclude that the method is successfully validated for O_3. The linear Mfit_s, derived from MOZAIC for O_3 between 5 and 11 km, is particularly suitable for filling Δ_f. Consequently, $\text{PTP}(O_3, z, t)$ and $\text{PTC}(O_3, t)$ may be derived without the use of data external to the MOZAIC data set.

To summarize, in order to provide the pure tropospheric profiles $\text{PTP}(O_3, z, t)$ when $z_{\text{top}} < z_s < z_{\text{DT}}$, we updated the methodology presented in Zbinden et al. (2006) by adding Mfit_s to $\text{TP}(O_3, z, t)$. The methodology was validated over three different sites, each located on a different continent, by using WOUDC coincident data sounding. We concluded that the seasonal cycles of the composite MOZAIC-WOUDC tropospheric columns were positively biased, always by less than 2 DU (6 %), compared to the MOZAIC pure tropospheric ozone column. This result allows to use this methodology on sites not documented by sondes. $\text{PTP}(O_3, z, t)$ and $\text{PTC}(O_3, t)$ at time t are finally estimated without any data external to the MOZAIC data set, which is a major advantage. Additionally, to obtain purely tropospheric columns for CO, a similar methodology is applied as 90 % of the column amount resides well below 12 km, with a maximum weight in the lowermost troposphere. Hereafter, in the text and the figures that follow, we will use $\text{MP}_s(X)$, $\text{TP}_s(X)$ or $\text{PTP}_s(X)$ for averaged profiles at season s and $\text{TC}_m(X)$ or $\text{PTC}_m(X)$ for averaged columns at month m and for a given molecule X, O_3 and CO.

4 Results

In this section, the methodology is applied to the 11 MOZAIC sites to derive three types of climatological products: (1) the monthly averaged pure tropospheric columns $\text{PTC}_m(X)$; (2) the seasonally averaged pure tropospheric profiles $\text{PTP}_s(X)$; and (3) the monthly averaged partial

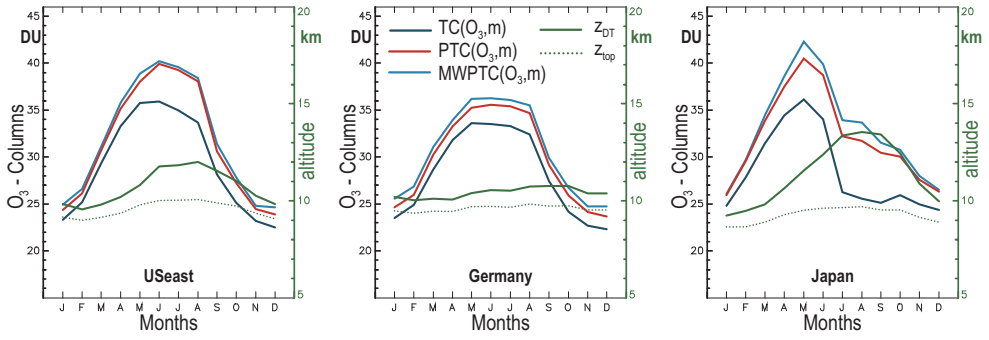

Fig. 4. Validation and impact of Δ on the pure tropospheric columns based on USeast, Germany and Japan seasonal cycles by comparing the following: $\overline{\mathrm{TC}}(\mathrm{O_3}, m)$, exactly what MOZAIC has measured in the troposphere (dark-blue line); $\overline{\mathrm{PTC}}(\mathrm{O_3}, m)$, the MOZAIC pure tropospheric ozone column (red line); and $\overline{\mathrm{MWPTC}}(\mathrm{O_3}, m)$, the composite MOZAIC-WOUDC tropospheric ozone column (blue line). All columns are expressed in DU. Δ is located between the altitude (in kilometres, right green vertical axis) given by the solid green line, the monthly average of z_{DT} in all cases, and the dotted green line, the monthly average of z_{DT} if $z_{\mathrm{DT}} < z_{\mathrm{top}}$ and z_{top} if $z_{\mathrm{DT}} > z_{\mathrm{top}}$.

columns, $\mathrm{BLC_m}(X)$, $\mathrm{MTC_m}(X)$ and $\mathrm{UTC_m}(X)$. Finally, $\mathrm{PTC_m}(X)$ is compared to satellite results.

4.1 Pure tropospheric column seasonal cycles

The $\mathrm{PTC_m}(\mathrm{O_3})$ and $\mathrm{PTC_m}(\mathrm{CO})$ cycles are given in Figs. 5 and 6, respectively. In Fig. 5, at all sites, the $\mathrm{TC_m}(\mathrm{O_3})$ cycles, the flat z_{top} and the z_{DT} are additionally provided. Over all months in Europe, the value of Δ is < 1.5 km. In contrast, Δ is up to 3 km in summer at the other sites, while in US-south and Uaemi it is between 1 and 4 km over all months due to intense domestic traffic. The numbers of monthly $\mathrm{O_3}$ profiles (1994–2009) and CO profiles (2002–2009) are given in Figs. 5 and 6, respectively. The best sampling rate is obviously over Germany. USeast, Paris, Vienna and Japan, still regularly visited, are sampled more than twice a week, which corresponds to the best ozonesonde sampling rate. Irregular visits over the 15 years lead to the lowest MOZAIC sampling frequency over Uaemi, Los Angeles and Eastmed. To further characterize the representativeness of sites, the figures also include statistics on inter-annual variability (IAV) with a box-and-whisker plot for the quartiles Q25, Q50 and Q75. No box means that only one month has been documented over the period.

4.1.1 Ozone seasonal cycle

Considering all the sites, $\mathrm{PTC_m}(\mathrm{O_3})$ varies from a European minimum of 23.7 DU in December to a Middle East maximum of 43.2 DU in July (Fig. 5). Below, we detail regional characteristics.

– The *European* $\mathrm{PTC_m}(\mathrm{O_3})$ *cycles* exhibit homogeneous patterns with a small summer maximum and a weak amplitude (i.e. from peak to peak here and thereafter) associated with a positive west–east gradient. Paris and Germany behave similarly, and $\mathrm{PTC_m}(\mathrm{O_3})$ are within 24.3 DU in winter and 35.6 DU in summer. Vienna differs slightly by reaching a summer maximum of 38.4 DU, probably due to its continental location and polluted air masses coming from the western part of Europe or the Po Basin (Baumann et al., 2001). As the z_{DT} variability is the weakest among the European sites (but also among all sites), the results obviously highlight the impact of photochemistry due to local or remote emissions of $\mathrm{O_3}$ precursors and long-range transport.

– The *Asian* $\mathrm{PTC_m}(\mathrm{O_3})$ *cycles*, i.e. Beijing and Japan, vary from 25–26 DU to 40–41 DU, with a strong similarity from December to May. We point out a strong regional contrast in June, when Beijing reaches a maximum and Japan declines sharply due to incoming $\mathrm{O_3}$-poor maritime air during the summer monsoon, consistent with what Logan (1985, 1999) reported from sonde analysis. In addition, z_{DT} over Japan is 2.5–5 km higher than over Beijing from July to September. Interestingly, of all the sites studied, Japan has the lowest amounts of summer $\mathrm{O_3}$ due to the impact of the monsoon. Thus, over Beijing, the higher CO compared to Japan (see Sect. 4.1.2), with probably higher $\mathrm{NO_x}$ (Lamsal et al., 2011), is favourable to higher $\mathrm{O_3}$ in July in spite of the summer monsoon. Note that Wang et al. (2012) reported far greater $\mathrm{O_3}$ tropospheric columns, up to 38 DU in winter and 70 DU in summer, over Beijing using sondes launched at 14:00 local time (LT) from 2002 to 2010 and taking the 2 °C $\mathrm{km^{-1}}$ lapse rate criterion for the tropopause. Firstly, their yearly averaged 46 DU, given for a 0–9 km partial column with a 4–5 % $\mathrm{yr^{-1}}$ increase, is far greater than our monthly summer maximum. Secondly, their monthly tropopause is located between 9 km (winter) and > 14 km (summer), 2 km above ours. Thirdly, their 140 to 600 ppbv monthly averaged $\mathrm{O_3}$ volume mixing ratios in summer, between 9 km and the tropopause, far

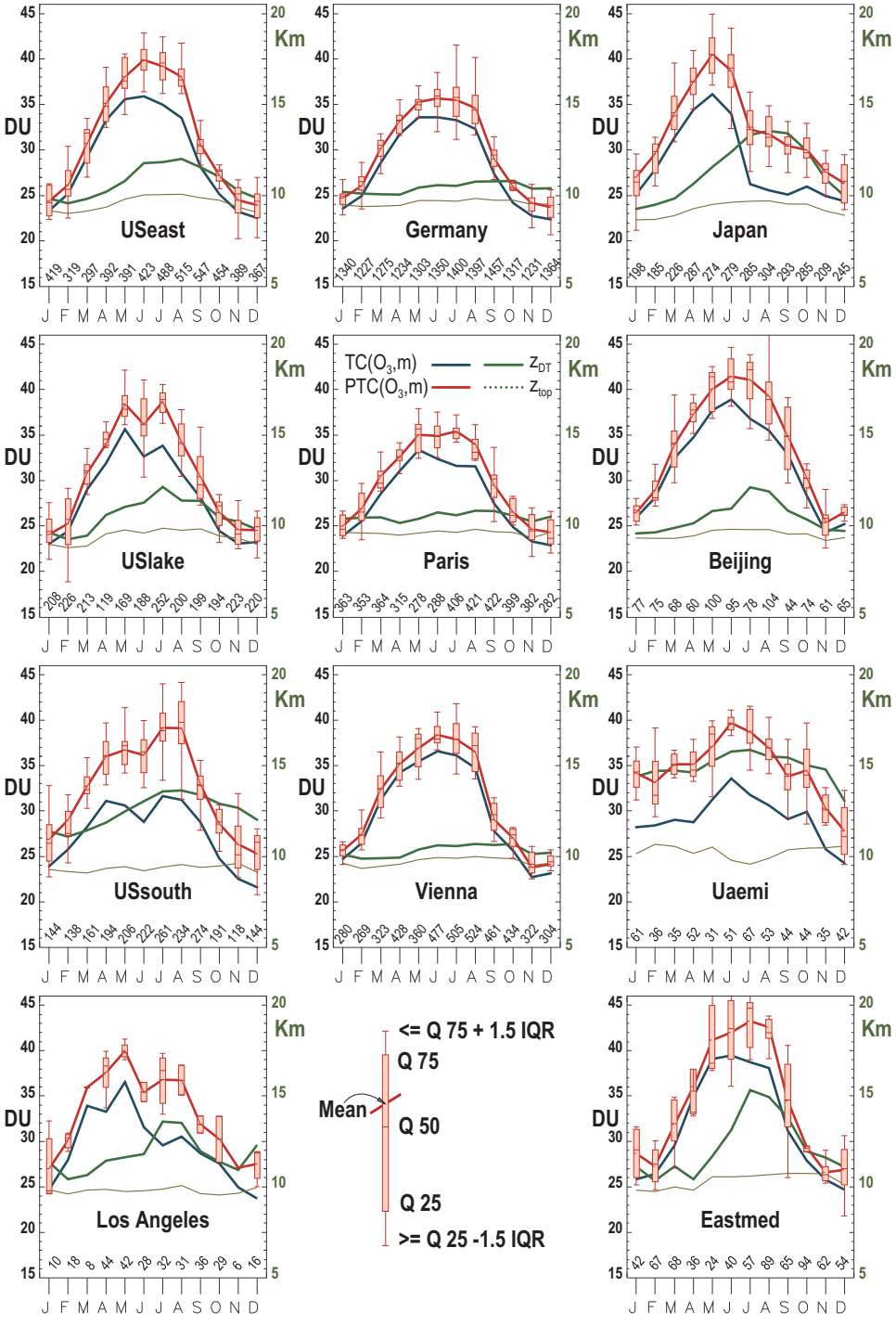

Fig. 5. Cycles of $TC_m(O_3)$, in blue, and $PTC_m(O_3)$ box-and-whisker plots, in red, expressed in DU by referring to left vertical axis for USeast, USlake, USsouth, Los Angeles, Germany, Paris, Vienna, Japan, Beijing, Uaemi and Eastmed. Δ is located between the altitude (in kilometres, right green vertical axis) given by the solid green line, the monthly average of z_{DT} in all cases, and the dotted green line, the monthly average of z_{DT} if $z_{DT} < z_{top}$ and z_{top} if $z_{DT} > z_{top}$. Monthly sampling frequency of each site is provided above the x axis. Box uses the quartiles [Q25, Q50, Q75]. The ends of the box-and-whisker plots are the $\geq$ Q25-1.5IQR or $\leq$ Q75+1.5IQR, where IQR is the interquartile range.

exceeds the 180 ppbv MOZAIC maximum at the same altitudes, suggesting a possible stratospheric air contamination. These combined factors obviously lead to much higher tropospheric columns than the pure tropospheric columns presented in our analysis.

– The *North American* $PTC_m(O_3)$ *cycles* show different patterns, from bimodal over the south (Los Angeles and USsouth), slightly bimodal over USlake, to perfectly unimodal over USeast. The z_{DT} variations probably contribute to the northern US cycle differences. The USeast cycle is close to that found in Europe despite a larger peak-to-peak range (24–40 DU (December–June)). The USlake cycle exhibits two maxima, in May and July (38 DU), with one local minimum in June (37 DU), surprisingly also detected at southern US sites. In the southern US, Los Angeles, rather poorly and irregularly monthly sampled (< 42 monthly profiles, March sampled only in 2005 and November only in 2004), shows two maxima (40 DU in May, 37 DU in July–August). The spring maximum, the biggest over the US, is related to the pollution transported from Asia (Jaffe et al., 2003, 2007; Parrish et al., 2004; Cooper et al., 2006, 2010; Brown-Steiner and Hess, 2011). In summer, the secondary peak appears rather small, despite a high z_{DT}, likely due to the strong influence of subtropical Pacific air masses, as Oltmans et al. (2008) have already shown. From the 24 h backward trajectories (provided on MOZAIC website), 50 % of the 1994–2006 profiles in summer reveal a subtropical Pacific air mass origin (36 % in May, not shown). In addition, during wintertime, the O_3 exceeds 27 DU in Los Angeles and is in the range of the Asian sites. This site is included in the study in spite of its poorest sampling, considered to be the lowest limit acceptable. The two modes of the USsouth seasonal cycle are inverted compared to Los Angeles, with 38.8 DU in April–May and 36.8 DU in July–August. The summer maximum of USsouth, highly enhanced compared to $TC_m(O_3)$ due to high z_{DT}, is now more consistent with the results reported by Cooper et al. (2006) and Li et al. (2005).

– The *Middle Eastern* $PTC_m(O_3)$ *cycles* show a high June–July maximum: 39.7 DU (Uaemi) and 43.2 DU (Eastmed). The Eastmed maximum is even larger than the Beijing maximum. Both appear to be in agreement with the summer extremes shown on the OMI/MLS[2] climatology produced by Ziemke et al. (2011). The Uaemi cycle is the flattest (11.9 DU amplitude) due to an extremely high and steady z_{DT} (> 14 km, except in December) and thus is greater than 33 DU from January to October. In contrast, the Eastmed cycle amplitude is 16.7 DU, the highest among all sites, associated with a 5 km z_{DT} amplitude. The difference between $TC_m(O_3)$ and $PTC_m(O_3)$ is less than 2 DU in spring compared to 4 DU in summer, where in the latter case the tropospheric column height has a significant contribution. In May, the $PTC_m(O_3)$ is more than 5 DU higher than Germany and is even higher than Beijing. These findings suggest favourable photochemical conditions allowing this local O_3 production, as detailed further in Sect. 4.2.3 and Fig. 9. In May, z_{DT} over Uaemi is 15 km (11 km) (Eastmed), while O_3 amounts are 37 DU (41 DU). Consequently, a high z_{DT} does not necessarily imply a high $PTC(O_3)$. Note that over Eastmed, the highest variability of all sites (7 DU interquartile range (IQR) in May and September) is linked to irregular monthly sampling. Despite sporadic regional sampling, MOZAIC contributes to the tropospheric-chemistry mapping of this area undocumented by ozonesondes.

This quasi-hemispheric overview of the $PTC_m(O_3)$ seasonal cycle shows an overall minimum in Europe, a summer maximum over the northeastern US, and a spring–summer maximum that is extreme in the Middle East and strong in Asia. The Asian summer monsoon results in an abrupt decline in June over Japan, unlike over Beijing, where pollutants such as CO, and probably NO_x, are exceptionally high, leading to a sharp geographical contrast in O_3. Furthermore, it is noteworthy that in summer, Japan exhibits the lowest pure tropospheric O_3 amounts of all the sites studied. The Asian–south-western US connection is highlighted in spring as Japan and Los Angeles $PTC_m(O_3)$ maximize. Over Uaemi, a high and rather steady z_{DT} strongly impacts the O_3 seasonal cycle, as seen in late winter and early spring, in contrast with Europe, where photochemistry, local emissions and long-range transport predominate. The European cycle patterns, very similar to those of the northern US, confirm a common source of variance. The low German IQR is related to the higher sampling quality and, quite likely, the low z_{DT} seasonal variability.

4.1.2 Carbon monoxide seasonal cycle

Here, we present another new result derived from MOZAIC. Figure 6 shows $TC_m(CO)$ and $PTC_m(CO)$ for all the sites with a scale change for Beijing to accommodate its high level of pollution. Because the CO measurements started later than O_3, in January 2002, the monthly sampling frequency is given in Fig. 6. Germany has the greatest sampling rate with at least 706 profiles per month, followed by Vienna (109–228), USeast (81–154), Japan (65–128) and USlake (43–162). The poorest statistical significance is in February over Beijing (no box-and-whisker plot) because this month is documented only in 2003. The Δ filling added to derive $PTC_m(CO)$ is less than 0.1×10^{18} molecules cm^{-2} over Europe and is greatest, $\sim 0.3 \times 10^{18}$ molecules cm^{-2} (16 %), over Japan and Uaemi in August. It is interesting to compare

[2] Ozone Monitoring Instrument/Microwave Limb Sounder.

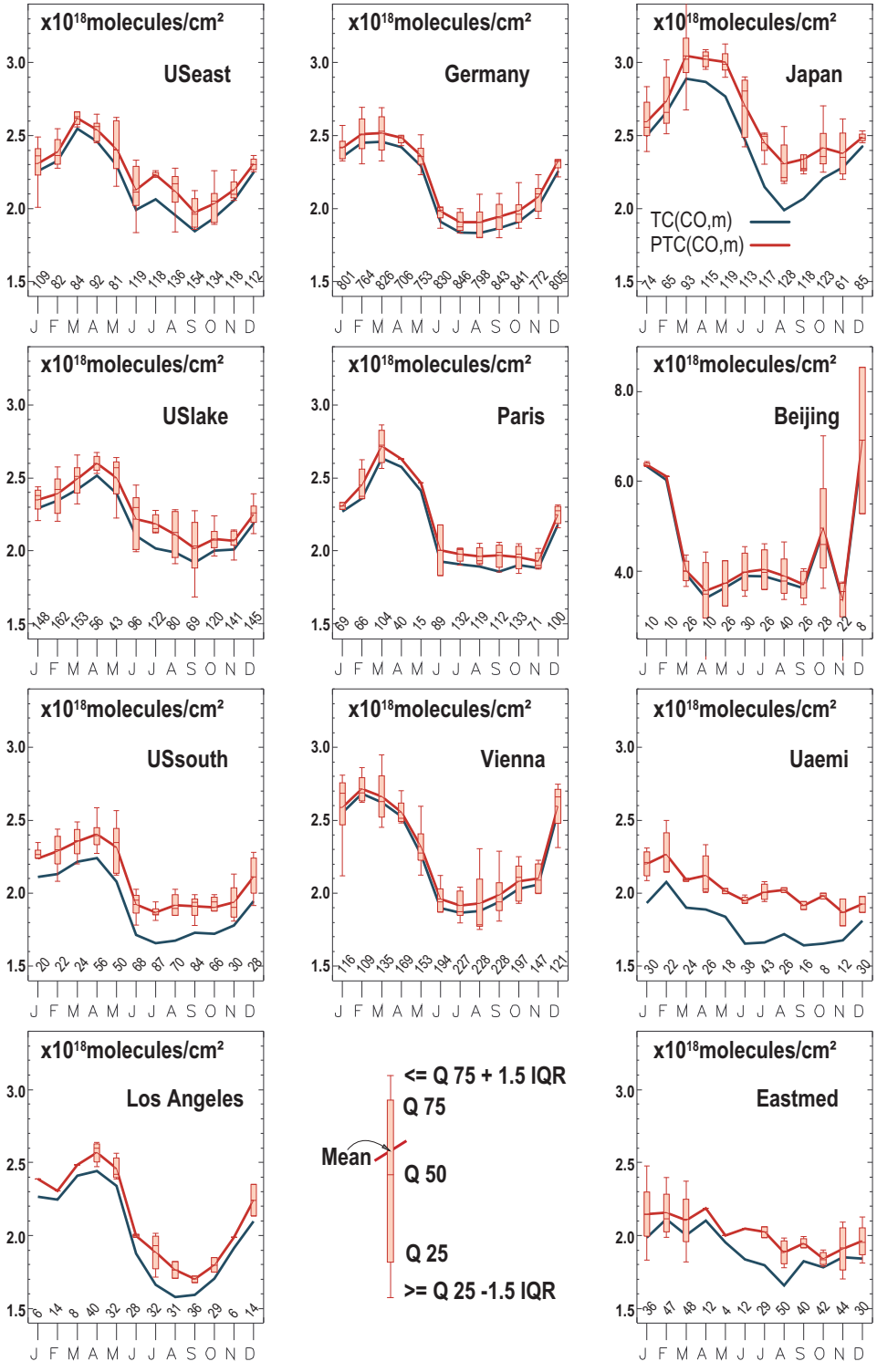

Fig. 6. Same as Fig. 5 but for CO, expressed in $\times 10^{18}$ molecules cm^{-2}. Note that only Beijing is plotted with a different scale.

Δ with the remote sensing errors, because, as far as we know, there is nothing equivalent to ozonesonde data to compare or validate with. SCIAMACHY[3] error range estimate of CO total columns (version 6.3) is 0.05–0.1 $\times 10^{18}$ molecules cm^{-2} (de Laat et al., 2007); ACE-FTS[4] (version 2.2) has $\sim$ 16 % bias on 108 MOZAIC coincidences between 5 and 12 km, where interfering species and temperature uncertainties have the strongest impact (Clerbaux et al., 2008); ACE-FTS (version 2.2) compared to SPURT aircraft data result in relative differences in the mean of $\pm$9 and $\pm$12 % in the upper troposphere and lower stratosphere, respectively (Hegglin et al., 2008), with an estimated 1 km vertical resolution; and MOPITT[5] (version 3) exhibits a positive bias at all altitudes, stronger at 750 hPa (25 %) than at 250 hPa (9 %) leading to a mean bias of 19 % on total column (Emmons et al., 2009). In a more recent study, from MOPITT, NOAA validation sites and the HIPPO[6] validation campaign, the bias, standard deviations, correlation coefficients and temporal drifts for the version 4, version 5-TIR and version 5-NIR have been estimated on the total column. The MOPITT bias with the NOAA validation sites are 0.07 $\times 10^{18}$ molecules cm^{-2}, 0.06 $\times 10^{18}$ molecules cm^{-2} and 0.08 $\times 10^{18}$ molecules cm^{-2}, respectively, with a noticeable temporal instrumental drift (Deeter et al., 2013). With the HIPPO validation campaign, the MOPITT bias in version 4 is 0.12 $\times 10^{18}$ molecules cm^{-2} and in version 5-TIR is -0.00×10^{18} molecules cm^{-2}. Thus, our Δ added to obtain PTC$_m$(CO) is less than or equivalent to remote sensing errors (except in cases of intense domestic traffic). At northern mid-latitudes, the PTC$_m$(CO) range is 1.7–6.9 $\times 10^{18}$ molecules cm^{-2}. All minima occur during June–November, and the maxima occur in early spring except in Vienna, Beijing, Uaemi and Eastmed, where they all occur in winter.

– The *North American* PTC$_m$(CO) *cycles* show an April maximum, except for USeast (March), and a September minimum, except for USsouth (July). Over all these sites, sharp May–June CO depletion highlights the powerful OH cleansing efficiency regulated by NO_x (Lamsal et al., 2010). The northern US cycles differ by less than 0.1 $\times 10^{18}$ molecules cm^{-2} and exhibit patterns more comparable to Europe than to any other sites due to the CO lifetime and strong connection through westerly winds. We found a July secondary peak over the USeast, associated with a small IAV, contrary to USlake. The IAV results from only 5 yr (2002–2006) for both northern US sites and, within this shorter period, the Canadian fires in 2004 (Turquety et al., 2007) were the most important fire events.

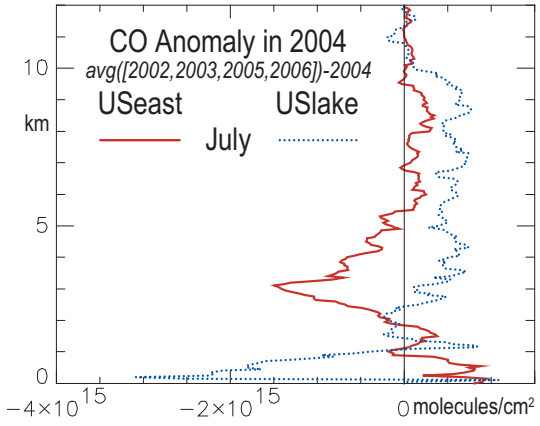

Fig. 7. Monthly mean tropospheric profiles of the CO July 2004 anomaly at USeast (red line) and USlake (dotted blue line) in molecules cm^{-2}.

The extension of Alaskan fires down to Texas on 18 July 2004 was pointed out by Morris et al. (2006) in a MOZAIC case study. These fires from Alaska and Yukon territories likely also extended to the west coast of the US. The profiles of the CO 2004 anomaly in July at USeast and USlake are given in Fig. 7. As a result, at USlake, there is a 2.5–10 km positive anomaly up to 0.8 $\times 10^{15}$ molecules cm^{-2} and a negative anomaly at USeast extending 2–5.5 km with a maximum at 3 km up to -1.6×10^{15} molecules cm^{-2}. Thus, this suggests that USeast was more on the CO plume pathway (or branch of pathway) than USlake. This finding and difference appear to be in agreement with what MOPITT has captured[7]. Fig. 7 also shows how negative and positive anomalies on profiles may be counterbalanced, leading to a lack of anomaly on PTC$_m$(CO) in 2004. Thus, the IAV of the PTC$_m$(CO) seasonal cycle cannot reveal such details. The two northern US sites show a June–October excess of CO (up to 0.3 $\times 10^{18}$ molecules cm^{-2}) compared to the southern US sites. USsouth shows a June–October-wide flat minimum, probably related to the pollution lifted under the influence of a semi-permanent anticyclone over Texas and the active summer convection that helps in lifting the surface pollution to the mid-troposphere (Li et al., 2005; Liu et al., 2006). The Los Angeles amplitude is 50 % greater than in the other US cycles. The winter–spring maximum is almost equivalent to that of the northern US sites, while the deep, narrow, low minimum in late summer probably suggests the impact of the depleted polluted air from Asia or clean air from the southern Pacific. Despite the poorest MOZAIC CO sampling, the seasonal cycle appears to be captured as well.

[3] SCanning Imaging Absorption spectroMeter for Atmospheric CHartographY.

[4] Atmospheric Chemistry Experiment Fourier Transform Spectrometer.

[5] Measurements Of Pollution In The Troposphere.

[6] HIAPER Pole to Pole Observations

[7] http://www.ucar.edu/news/releases/2005/wildfires.shtml

– The *European* $PTC_m(CO)$ *cycles* vary from 1.9 to 2.7×10^{18} molecules cm^{-2}. The IQR over Germany are the steadiest, with for all of them less than 0.25×10^{18} molecules cm^{-2}, and highlight the impact of the sampling frequency that is well illustrated by comparing the three European sites in June. The sharp depletion in May–June, already seen over the US, is evidence of the powerful OH cleansing efficiency regulated by NO_x (Lamsal et al., 2011). Later, the seasonal cycle remains almost unchanged from June to November (Paris) or starts a very slow increase in August (other European sites), probably related to remote fires. Interestingly, wintertime shows higher amounts over Vienna than over Paris (10 %) or Germany because of its downwind position in Europe or the influence from the Po Valley.

– The *Middle East* $PTC_m(CO)$ *cycles* are both in the same range. They show the lowest $PTC_m(CO)$ in winter and the comparable weakest seasonal cycle amplitudes ($1.8–2.3\times10^{18}$ molecules cm^{-2}). Focusing on Dubai, Tangborn et al. (2009) compared MOZAIC to the assimilated SCIAMACHY CO data into the Global Modeling and Assimilation Office (GMAO), which includes the CO transport by the use of meteorological analyses from the Goddard Earth Observing System (GEOS) version 4. From this comparison, with favourable cloud-free conditions, they had to reduce the OH by 10 % and double the CO emissions in the model in order to lessen the total CO column differences to their MOZAIC independent data set from 1.0 to 0.6×10^{18} molecules cm^{-2}. Nevertheless, their MOZAIC data set did not take into account the extremely large unvisited tropospheric remainder, which we estimated to be ~ 10 % of $PTC_m(CO)$ as a yearly average performed in 2004 and greater than 0.3×10^{18} molecules cm^{-2} in October, i.e. equivalent to the amplitude of the seasonal cycle. Over Eastmed, due to the spring low $PTC_m(CO)$ in May–June, CO does not appear to be the most important spring source of O_3 here, and thus the large amount of $TC_m(O_3)$ appears here to be more consistent with intense stratosphere–troposphere exchanges (STE), NO_x contribution or a long-range transport hypothesis. In summer, CO remains in the same range as over Europe, far less than in Asia.

– The *Asian* $PTC_m(CO)$ *cycles* exhibit the highest CO amounts. They are extremely favourable to O_3 production when combined with the highest NO_x amount on the hemisphere scale as detected from satellites over China, during 1996–2005, and related to human activity (van der A et al., 2008; Schneider and van der A, 2012). The Beijing CO cycle in Fig. 6 has a very different vertical scale of 2.5–9.0×10^{18} molecules cm^{-2}. In fact, the minimum of its cycle is 3.35×10^{18} molecules cm^{-2} in November, and this minimum exceeds the maximum of all the cycles of the 10 other sites studied (i.e. 3.05×10^{18} molecules cm^{-2} in March in Japan). These highest values are associated with the largest inter-annual variability (see Beijing – in December with 10 profiles sampled) and we noted that Beijing in February was only sampled in 2003 (no box-and-whisker plot). The Japanese cycle peaks in March (3.0×10^{18} molecules cm^{-2}) reaches a minimum in August (2.3×10^{18} molecules cm^{-2}) and has an irregular IQR from 0.1 to 0.4×10^{18} molecules cm^{-2}. Finally, regardless of season and prevailing winds considered, the air masses over Beijing are systematically CO-enriched by a factor of 1.2–2.8 compared to Japan.

4.2 Pure tropospheric profiles

To complement the tropospheric column climatology, the $PTP_s(O_3)$ and $PTP_s(CO)$ are provided to evaluate the vertical anomalies more precisely from a regional point of view. The North American, European, and the Asian and Middle Eastern sites are grouped together in Figs. 8, 10 and 11, respectively. The $PTP_s(X)$ are plotted up to the seasonal mean z_{DT} between 9.5 and 15 km. This additional information along the vertical allows for further analysis, shedding light on the origin of the two chemical species. For this reason, the O_3 (top row) and CO (bottom rows, i.e. 0–2 km and 2–15 km) are on the same figure for each region.

4.2.1 North American profiles

The results are plotted in Fig. 8. Over the northern US, the $PTP_s(O_3)$ show the typical autumn–winter and spring–summer seasonal dichotomy as previously described in Zbinden et al. (2006). This is the typical seasonal behaviour of the vertical pure tropospheric ozone distribution in northern mid-latitudes. It characterizes the photochemical activity leading to O_3 production. The $PTP_s(CO)$ presents a different dichotomy in the free troposphere with a winter–spring maximum and a summer–autumn minimum, the minimum probably being related to the higher amounts of OH at that time. Over the southern US, the seasonal vertical distributions are slightly different. Over USsouth, between 1 and 4 km, the summer O_3 profile reveals the O_3-poor monsoon flux impact. Among all the sites, we found the lowest amounts of CO here in the summer BL because the high OH amounts shortened its lifetime. Between 6 and 9 km, quantities of O_3 are enhanced, probably due to additional O_3 from lightning NO_x production, especially in summer (Li et al., 2005). This counterbalances the low amounts of O_3 in the BL and explains why the tropospheric columns in summer are still maximized (Fig. 5). In autumn, the amounts of O_3 in the BL are higher than in winter and thus the typical dichotomy is strongly modified. Furthermore, at that time in the BL, the CO is the lowest of all the studied sites likely due to the influence of

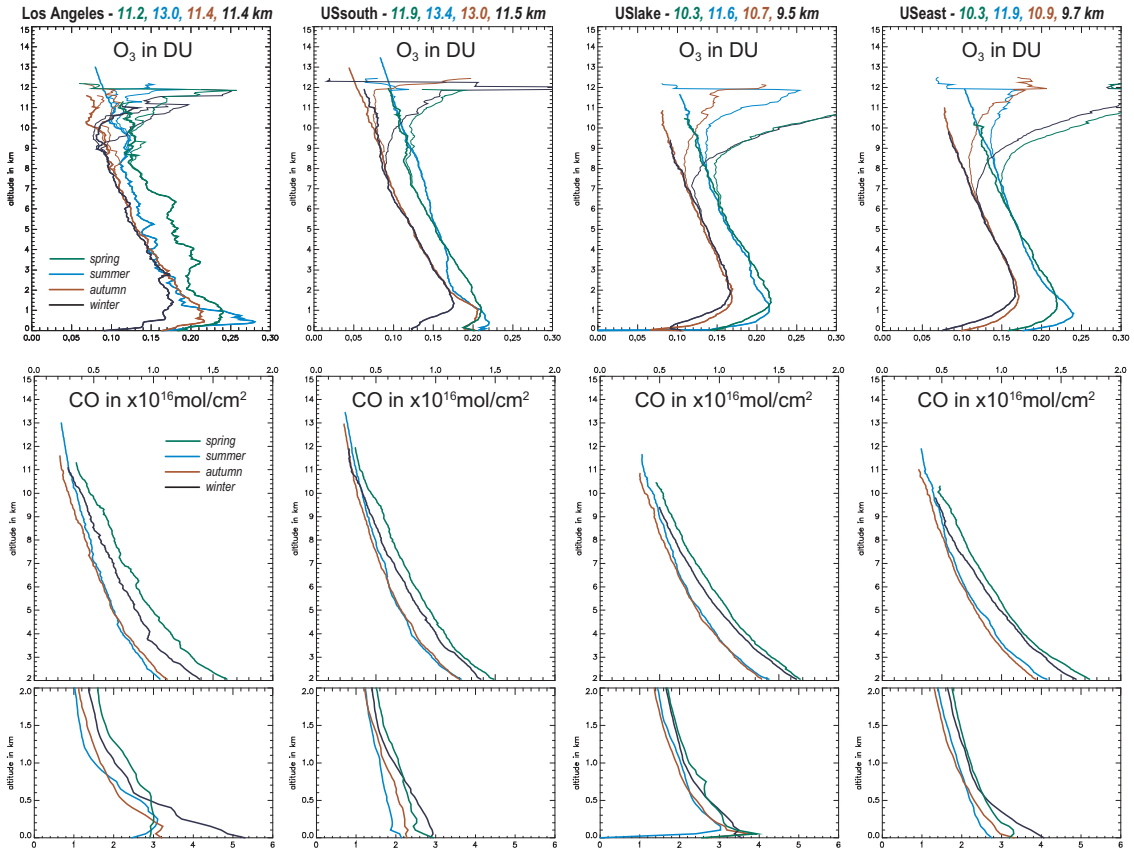

Fig. 8. Seasonal profiles for O_3 and CO (top and bottom) over Los Angeles, USsouth, USlake and USeast (left to right). For O_3, $MP_s(O_3)$ are the thin lines and $PTP_s(O_3)$ are the thick lines limited to the seasonal z_{DT} and expressed in DU. The CO includes only the $PTP_s(CO)$, expressed in $\times 10^{16}$ molecules cm^{-2}, using different horizontal scales and two vertical scales for altitude (0–2 km bottom, 2–15 km top). The spring, summer, autumn and winter profiles are in green, blue, brown and black, respectively. The seasonal z_{DT} are given using the seasonal colours on the top of each site plot in kilometres.

oceanic air masses. Thus, this suggests this BL high ozone results from very local production, in which biogenic emissions might interplay. Note that airborne measurements over the southern United States during the field campaigns TexAQS2000, ICARTT2004 and TexAQS2006 have allowed for quantifying the biogenic emissions, have shown great interannual variability (by a factor of 2) within the period 2002–2006, and have found that the emission inventories were overestimated by a factor of 2 (Warneke et al., 2010). The biogenic emissions contribution is a hypothesis to explain this higher ozone in the BL. Such characteristics are also observed over Los Angeles and Beijing (see below). With regard now to Los Angeles, the typical autumn–winter and spring–summer seasonal dichotomy is not found, and this change cannot be attributed to the poor sampling because Germany, when under-sampled consistently with Los Angeles in coincidence (within 24 h), still shows the seasonal dichotomy (Fig. 9). The Los Angeles profiles in Fig. 8 exhibit fine structures along the vertical, probably accentuated by the low MOZAIC monthly sampling rate. However, the spring O_3 spikes of +0.03 DU between 2 and 7 km could be indications of long-range transport from Asia (Jaffe et al., 2003; Parrish et al., 2004; Cooper et al., 2005; Neuman et al., 2012). Above 1 km, the summer O_3 profile is unusually close to the autumn–winter one (less than 0.02 DU difference), while the CO profile is extremely low, which might be related to air coming from the southern Pacific, as already studied by Oltmans et al. (2008) and Neuman et al. (2012). In contrast, below 1 km, the highest summer maximum of all the sites studied (0.28 DU) seems to be more in agreement with the lack of deep convection (Cooper et al., 2006). The winter CO below 0.5 km is higher than elsewhere in the US. Thus, to summarize from what MOZAIC has measured under these poor sampling conditions, the secondary peak of the $PTC_m(O_3)$, in summer, depends on a high z_{DT} and on heavy local pollution as O_3 in the BL reaches 0.28 DU (maximum of the overall study) with high CO up to 3×10^{16} molecules cm^{-2}.

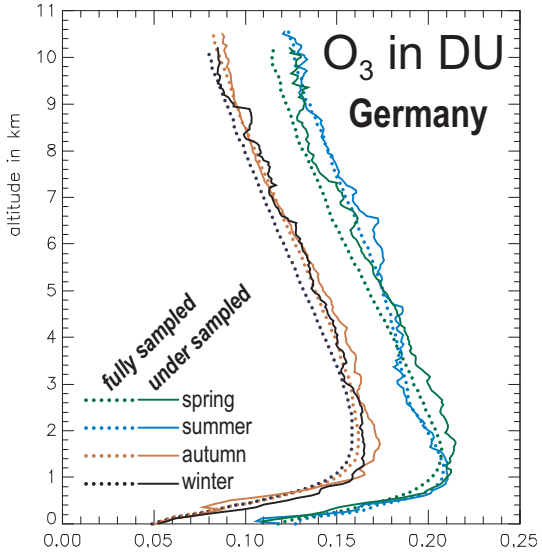

Fig. 9. Seasonal tropospheric O_3 profiles for Germany as sampled by MOZAIC (16 041 profiles, plain lines) and under sampled consistently with the Los Angeles (300 profiles, dotted lines) in 24 h coincidence.

4.2.2 European profiles

The European O_3 profiles (Fig. 10) present similar seasonal dichotomies and are comparable to the two northern US ones (Fig. 8). Nevertheless, we found the following: (1) O_3 excess all throughout the troposphere explains the higher $PTC_m(O_3)$ over Vienna compared to the other European sites; (2) the greatest spring CO amounts above 2 km over Paris are indications of long-range pollution transport by the westerly wind from the east coast of the US; and (3) during winter, in the BL, CO increases from west to east, suggesting strong contamination by dry CO-polluted air from central and eastern Europe, in agreement with Kaiser (2009). The influence of the Po Basin on Vienna might be another source of contamination, but it is currently difficult to quantify (Kaiser, 2009); (4) over Vienna, regardless of season, at the surface, O_3 and CO are at least 10 ppbv and 25–50 ppbv greater than at the other European sites (not shown), again evidence of higher pollution.

4.2.3 Middle Eastern and Asian profiles

The seasonal profiles for the Middle East (Eastmed and Uaemi) and Asia (Beijing and Japan) are given in Fig. 11. Interestingly, none of them has the typical seasonal O_3 and CO dichotomy as seen over Europe or the northern US. For O_3, this is due to (1) a strong positive summer 1–7 km anomaly over Eastmed; (2) a spring profile closer to autumn–winter over Uaemi above 2 km compared to all the other sites; and (3) strong summer anomalies in Asia. Note the CO horizontal scale change for the 2–15 km range over Beijing and Japan and the 0–2 km range over Beijing (by a factor of 6).

Over Middle Eastern sites, very similar winter profiles above 1 km for O_3 and CO suggest a probable common source of variance. Thus, the $PTC(O_3)$ seasonal cycle contrast in winter comparing the two sites (Sect. 4.1.1) is mainly due to z_{DT}. The Eastmed autumn profile is above 3 km in the range of Europe and less than Uaemi, while below 3 km, Eastmed exceeds Uaemi and of course Europe. At that time and below 3 km, a minimum of O_3 and CO over Uaemi might be related to the impact of sea breezes at the surface (Eager et al., 2008) and OH efficiency. Lawrence and Lelieveld (2010) reported evidence of a broad summertime Middle East O_3 maximum around 400–500 hPa. The authors mentioned this O_3 anomaly is "in contrast to the ozone-depleted Asian airmasses observed in the upper troposphere during MINOS, and is not always observed in satellite retrievals (e.g., Fishman et al., 2003; Liu et al., 2006)" and that "the cause of this difference is not yet resolved". Therefore, it seems useful to comment on the MOZAIC summer profiles in more detail. At 6 km, at both Middle Eastern sites, the O_3 and CO amounts are similar and O_3 is identical to that of Beijing and greater than in Europe. Above 6 km, the O_3 profiles are still comparable but surprisingly lower than Europe or Beijing (by 0.02 DU at 9 km), which suggests STE are probably not the most predominant processes involved. Below 6 km, the O_3 profiles show a marked contrast, as follows: (1) over Eastmed, an intense O_3 maximum within 1–6 km, never reached elsewhere in our study, and (2) over Uaemi, a pronounced negative O_3 anomaly (by -0.06 DU at 3 km) with higher amounts of CO ($+10$ %) when compared to Eastmed. The strong O_3 and CO anomalies combined with high levels of H_2O (not shown) over Uaemi exclude the impact of predominant STE and probably reveal an intense inflow of sea air and an influence of the remote Indian summer monsoon, in agreement with Li et al. (2001). Lastly, in spring, the Uaemi O_3 profile is unusually close to autumn and winter profiles, in particular at 3 km. These results are in good agreement with the summer extremes shown on the OMI climatology produced by Ziemke et al. (2011) and with the Persian Gulf region study by Lelieveld et al. (2009). The summer O_3 at 5–7 km agrees well with the model results from Liu et al. (2011) and the study of Lelieveld et al. (2009). Liu et al. (2011) emphasize that the geographic position of the Arabian anticyclone has a major influence on chemical transport. They show that the Middle East mid-tropospheric summer maximum is strongly related to Asian sources of pollution (> 30 %), to local production (23 %) and also to northern USA pollution (> 6 %) transported through the subtropical westerly jet that descends in this area. Over the Zagros Mountains, using spaceborne SAGE II[8] data, Kar et al. (2002) found a CO summer positive anomaly at 7 km over 1985–1990 and 1994–1999 and, in a 2003 spaceborne MOPITT study, argued and explained it as thermal mountain winds venting the BL (Kar et al., 2006). We found a different

[8]Stratospheric Aerosol and Gas Experiment II.

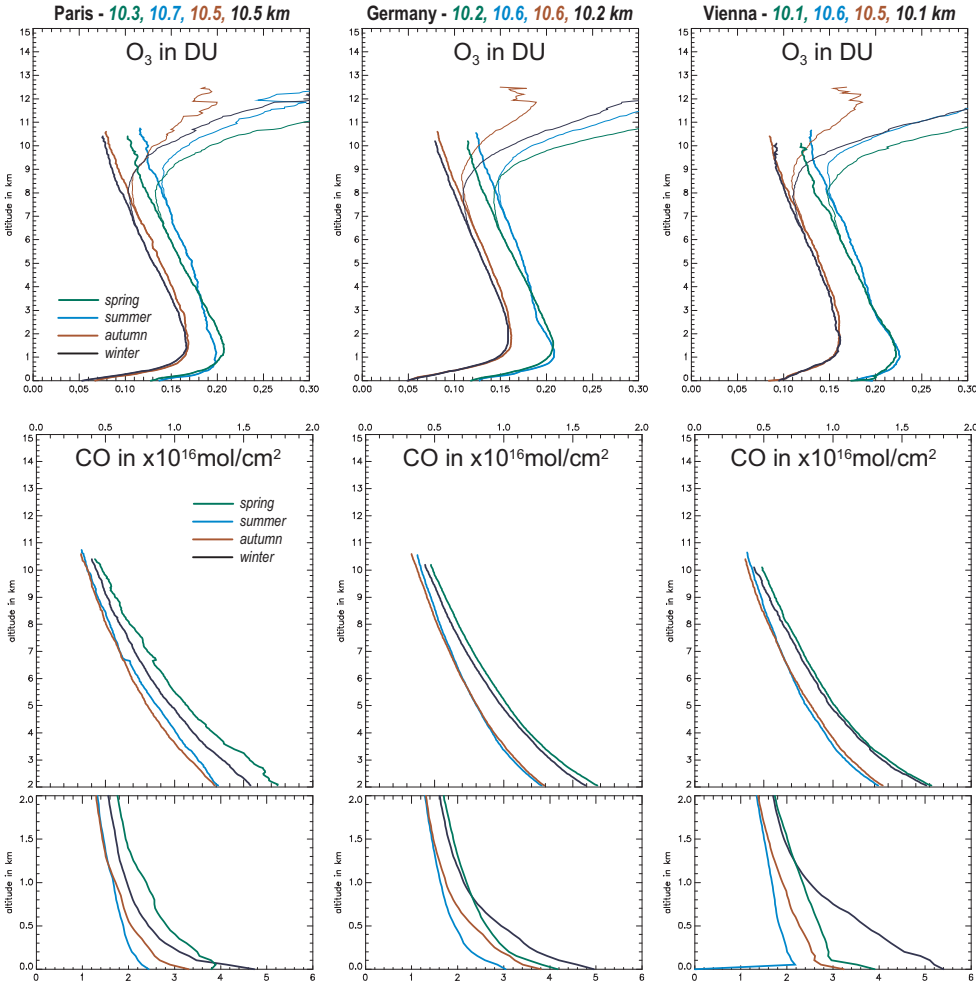

Fig. 10. Same as Fig. 8 but for Paris, Germany and Vienna.

notable summer positive (negative) CO anomaly at Uaemi within 3–6 km (at 7 km) and not over Eastmed, with the MOZAIC sampling conditions and period. Due to regional complexity, extensive work is needed in order to go further into the geographical and seasonal variabilities, and in future studies we deeply recommend the addition of the H_2O climatology using MOZAIC/IAGOS to reinforce the hypothesis on processes involved and air mass origin.

Over Asia (Fig. 11), a comparison of Japan and Beijing seasonal O_3 profiles reveals that (1) winter and spring profiles are very similar, with a difference of less than 0.01 DU; (2) the autumn Beijing profile exceeds Japan by 0.03 DU (only 0.01 DU) in the BL (at 8 km); and (3) the summer Beijing profile exceeds Japan by 0.10 DU (0.02 DU) in the BL (at 8 km); and thus in Japan, O_3 at 2 km is reduced to the minimum ever seen regardless of season. Interestingly, up to 4 km, Japan has less CO in all seasons than Beijing by a factor of 2–8, but above 4 km, the two profiles are similar ($< 0.2 \times 10^{16}$ molecules cm^{-2}), suggesting a common source of variance. The Beijing winter CO maximum is extremely large, exceeding 30×10^{16} molecules cm^{-2} or 1800 ppbv in the BL (Japan is 4.2×10^{16} molecules cm^{-2} or 220 ppbv, even less than Vienna). A comparison of the two sites highlights the prevailing wind mechanism and the predominant monsoon impact. Both sites show a summer O_3 depletion below 5 km, but the monsoon is (1) less efficient over Beijing, probably due to the high CO (10×10^{16} molecules cm^{-2} at the surface) compared to Japan, and (2) so intense over Japan that below 4 km, O_3 summer amounts are less than in winter. The monsoon is the most important and powerful mechanism for reducing tropospheric O_3 on the hemispheric scale.

The pure tropospheric column and profile climatologies of O_3 and CO presented in this study are complementary, highlighting seasonal variability and vertical anomalies and reinforcing the hypothesis on the processes involved in the northern mid-latitudes. The pure tropospheric profiles obtained here are significantly different from atmospheric profiles above 6 km. The autumn–winter and spring–summer seasonal O_3 dichotomy characterizes the typical seasonal behaviour of the vertical pure tropospheric ozone distribution in

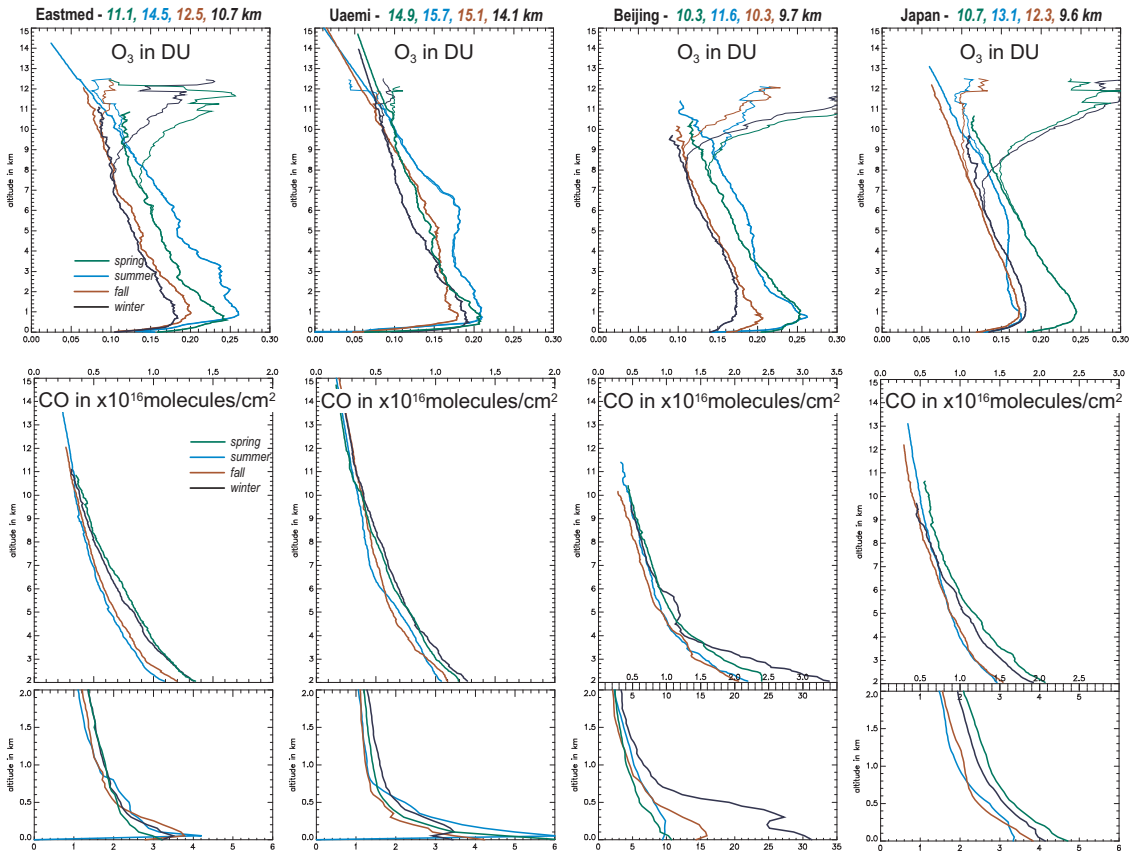

Fig. 11. Same as Fig. 8 but for Eastmed, Uaemi, Japan and Beijing, from left to right. Note that for CO, the horizontal scale changes exclusively for Beijing in the 0–2 km section of the graph, and for both Japan and Beijing in the 2–15 km section of the graph.

the northern mid-latitudes. It characterizes the photochemical activity leading to O_3 production. The CO dichotomy, not so obvious and different to the O_3 dichotomy, is pointed out with a winter–spring maximum and a summer–autumn minimum in the free troposphere. The minimum is related to the higher amounts of OH at that time. We have singled out the monsoon as the most efficient regime for O_3 reduction, with a significant impact on the hemispheric scale in the northern mid-latitudes, below 6 km. Such a pure tropospheric climatology should be considered as a reference for validation remote sensing instruments or chemistry–transport model outputs.

4.3 Partial tropospheric columns

Here, we investigate the interest of characterizing z_{Ld}, the altitude from which $\mathrm{PTP_m}(X)$ and $\mathrm{MP_m}(X)$ diverges, to calculate the BL, MT and UT partial tropospheric columns (BLC, MTC and UTC, respectively) for USeast, Germany and Japan.

4.3.1 Divergence between MP and PTP

The limit, z_{Ld}, is defined by month, and examples are given in Fig. 2a. z_{Ld} varies by season and site due to either tropopause altitude variations or the occurrence of stratospheric air detection. The z_{Ld} is higher in summer than in winter and generally higher at southern sites than at northern sites. For example, the 6 km minimum of z_{Ld}, observed in late winter over USeast, is an indication of high residence frequency of the polar jet stream and a low tropopause. In August, over USeast the z_{Ld} is 9.5 km; therefore the MT ceiling fixed at 8 km, as used in Zbinden et al. (2006), is not satisfactory. We suggest replacing it with the monthly varying one, z_{Ld}, defined as the lowest altitude where $\mathrm{MP_m}(O_3)$ differs from $\mathrm{PTP_m}(O_3)$ by 0.001 DU. In this way, UT, the layer between z_{Ld} and z_{DT}, strongly influenced by the stratosphere–troposphere transients, will be more faithfully represented by month.

The z_{Ld} seasonal cycle varies in a 6–12 km range (Fig. 12). Due to low variability of the z_{DT} over Germany, z_{Ld} varies less (6.6–8.1 km) than USeast (6.0–9.5 km) or Japan (6.0–11.9 km). In Thouret et al. (2006) the tropopause layer has been defined between $z_{\mathrm{DT}} - 15$ hPa and $z_{\mathrm{DT}} + 15$ hPa, with

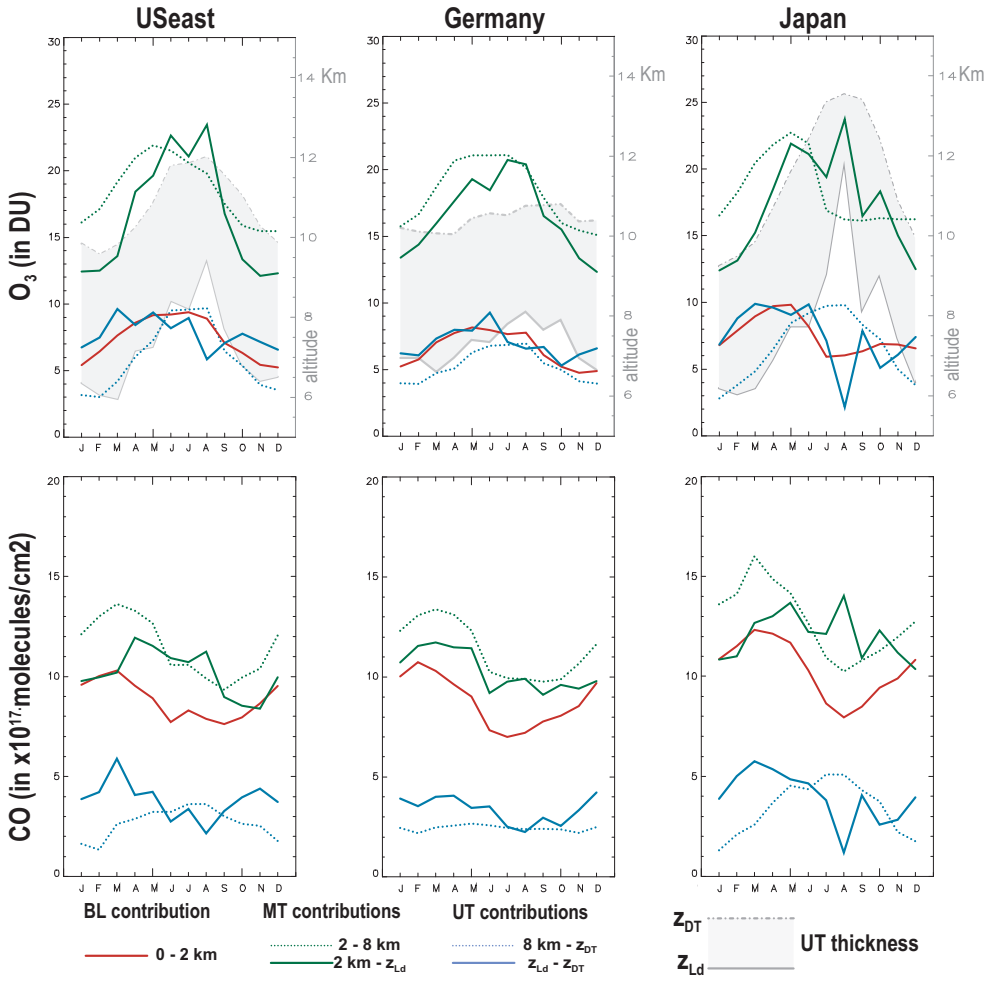

Fig. 12. Tropospheric partial columns: $BLC_m(O_3)$ (red), $MTC_m(O_3)$ (green) and $UTC_m(O_3)$ (blue) for USeast, Germany and Japan (left to right). The previous MTC_m [2–8 km] and UTC_m [8 km–z_{DT}] are the coloured dotted lines and, by using monthly varying limits, the new MTC_m [2 km–z_{Ld}], and the UTC_m [z_{Ld}–z_{DT}] results are the coloured thick lines. O_3 (top row) and CO (bottom row) are expressed in DU and in molecules cm^{-2}, respectively. The shaded areas in the O_3 plots highlight the UTC thickness (between z_{DT} and z_{Ld}, the dotted dashed line and the grey line, respectively), referring to the right vertical scale in kilometres.

z_{DT} fixed at 2 PVU. Our UTC thickness, shown only with respect to altitude in Fig. 10, is in the range of 115–170 hPa, 52–214 hPa and 45–194 hPa for Germany, USeast and Japan, respectively. Therefore, in contrast to the tropopause layer, our UTC is much thicker and excludes the stratospheric air above z_{DT}. Moreover, our UTC is thicker in winter than in summer (Fig. 12) and z_{Ld} highlights the lowest winter tropopause position in the northern mid-latitudes. This finding is noteworthy because the seasonality of the deepest stratospheric intrusions, the one that stayed more than four days in the troposphere, is characterized by a winter maximum and a summer minimum (Stohl et al., 2003). Finally, as dynamical and photochemical processes are different in the BL, MT and UT, we give the O_3 and CO partial tropospheric columns over USeast, Germany and Japan using either the steady altitude fixed at 8 km or a monthly varying z_{Ld} used as the MT ceiling (Fig. 12). The partial tropospheric columns using z_{Ld} have been evaluated strictly for those three most documented sites in order to present significant results, and not elsewhere. The results are summarized in Table 4. No major change in BL is expected with respect to Zbinden et al. (2006) given that the small variations depend only on the time period update.

4.3.2 BL, MT and UT seasonal cycles

The $BLC_m(O_3)$, the $MTC_m(O_3)$, and the $UTC_m(O_3)$ range from 4.8 to 9.8, 12.1 to 23.8 and 2.2 to 9.9 DU, respectively (Fig. 12). Thus, using fully defined MOZAIC tropospheric columns and z_{Ld}, $UTC_m(O_3)$ are enhanced by 2 DU and show smaller amplitudes than those in Zbinden et al. (2006). Interestingly, the $UTC_m(O_3)$ maximum is shifted from summer to late winter–early spring. This may be observed even

Table 4. Pure tropospheric columns PTC(X, s) and related partial columns, UTC(X, s), MTC(X, s) and BLC(X, s), where X is O_3 and CO at season s over USeast, Germany and Japan in DU and in $\times 10^{18}$ molecules cm^{-2}, respectively. These results are in bold. For O_3, the additional small numbers/letters in parentheses refer to previous values on incomplete tropospheric columns (TOC) and partial columns as given in Zbinden et al. (2006). MTC and UTC (bold) are derived using the new L_d definition.

		USeast				Germany				Japan			
		Spring	Summer	Autumn	Winter	Spring	Summer	Autumn	Winter	Spring	Summer	Autumn	Winter
O_3	(TOC)	(33.4)	(37.8)	(26.8)	(24.0)	(32.0)	(34.0)	(25.1)	(23.9)	(36.1)	(31.5)	(27.5)	(26.4)
	PTC	**34.82**	**39.24**	**27.68**	**25.05**	**33.05**	**35.31**	**26.55**	**24.97**	**37.60**	**34.52**	**29.66**	**27.44**
	(UTC)	(5.7)	(8.1)	(4.8)	(3.8)	(5.3)	(6.2)	(4.2)	(4.0)	(5.9)	(7.2)	(5.0)	(3.5)
	UTC	**9.14**	**7.67**	**7.34**	**6.93**	**7.76**	**7.64**	**6.05**	**6.31**	**9.54**	**6.37**	**6.34**	**7.68**
	(MTC)	(20.0)	(20.3)	(16.2)	(15.6)	(19.6)	(20.3)	(16.0)	(15.3)	(21.3)	(17.8)	(16.1)	(16.4)
	MTC	**17.21**	**22.40**	**14.08**	**12.41**	**17.63**	**19.86**	**15.13**	**13.37**	**18.56**	**21.43**	**16.61**	**12.69**
	(BLC)	(8.3)	(9.4)	(6.2)	(5.4)	(7.5)	(7.7)	(5.1)	(5.0)	(9.5)	(6.4)	(6.6)	(7.1)
	BLC	**8.47**	**9.17**	**6.27**	**5.70**	**7.66**	**7.81**	**5.37**	**5.30**	**9.50**	**6.72**	**6.70**	**7.08**
CO	**PTC**	**2.55**	**2.17**	**2.06**	**2.35**	**2.50**	**1.96**	**2.04**	**2.47**	**3.05**	**2.50**	**2.39**	**2.61**
	UTC	**0.47**	**0.28**	**0.39**	**0.39**	**0.38**	**0.28**	**0.29**	**0.39**	**0.53**	**0.32**	**0.32**	**0.43**
	MTC	**1.12**	**1.10**	**0.86**	**0.99**	**1.15**	**0.96**	**0.94**	**1.07**	**1.31**	**1.28**	**1.15**	**1.07**
	BLC	**0.96**	**0.80**	**0.81**	**0.97**	**0.97**	**0.72**	**0.81**	**1.02**	**1.21**	**0.90**	**0.93**	**1.11**

over Germany, where the z_{DT} and z_{Ld} variations are the lowest. In August, the use of z_{Ld} over Japan needs to be regarded with caution due to the low sampling rate of the upper-tropospheric layers. Besides the $UTC_m(O_3)$ shift, we also highlight the intense vertical expansion of $MTC_m(O_3)$. Thus, over Japan, the previous obvious spring $MTC_m(O_3)$ maximum has turned into a pronounced summer maximum because the O_3-poor air mass due to the monsoon in the lower mid-troposphere is balanced by the high column height.

The BLC_m(CO), the MTC_m(CO) and the UTC_m(CO) range from 0.7 to 1.1, 0.9 to 1.4 and 0.1 to 0.6 $\times$ 10^{18} molecules cm^{-2}, respectively. The BLC_m(CO) of the three sites show an increase in amounts and amplitudes from west to east, with a late winter/early spring maximum and a summer minimum.

Even over Germany, where the seasonal z_{DT} is very flat, in MTC_m and UTC_m, the cycles and amplitudes change when the monthly varying z_{Ld} is used instead of a fixed 8 km altitude. This change becomes significant over USeast and Japan and is obviously linked either to the reservoir thickness or the O_3 amounts. The spring O_3 maximum in MT observed using a fixed 8 km altitude has turned into a broad April–August maximum using z_{Ld}, and UT has become out of phase with an overall August minimum and spring maximum.

4.4 Comparison with spaceborne measurements

Our aim in this last section is not to validate satellite products but to demonstrate the benefits of such pure tropospheric climatology based on MOZAIC fully defined individual tropospheric columns. Thus, we compare our new O_3 and CO pure tropospheric columns with the publicly available remote sensing results from the Giovanni website (http://disc.sci.gsfc.nasa.gov/giovanni) on a monthly average basis. The seasonal cycle comparison between the spaceborne and MOZAIC data is performed using the TES level-3 version 2 (2.0° × 4.0° gridded data) and AIRS level-3 version 5 (1.0° × 1.0° gridded data). Our PTC(O_3) will be compared to the tropospheric O_3 columns from TES[9] (Beer et al., 2001, Worden et al., 2007) by selecting the periods 2006–2007 or 2007. Our PTC(CO) will be compared to the CO columns from AIRS[10] (Susskind et al., 2003, 2010) by selecting the 2002–2009 period. We focus only on two sites because of their contrasting z_{DT} seasonal cycle: Germany [47–52° N, 6–10° E] and Japan (Fig. 13), and separately providing Tokyo [35.6–37.6° N, 138.7–140.7° E], Nagoya [34.1–36.1° N, 135.8–137.8° E] and Osaka [33–35° N, 134–136° E] to also check the consistency of the individual sites. Our comparison is indeed not a validation. Validation has to be strictly truly one to one, like in Worden et al. (2007) for TES O_3 and in McMillan et al. (2011) for AIRS CO. Nevertheless, the simple comparison we provide here is interesting by itself because it results from two independent data sets, with their own limit and performance.

4.4.1 Ozone

First of all, the recent O_3 tropospheric climatology study from Ziemke et al. (2011) merits consideration. It combines OMI/MLS measurements over six years (2004–2010). Interestingly, on two regions not sampled by ozonesondes, OMI/MLS results in Ziemke et al. (2011) are in agreement with (1) the MOZAIC tropospheric seasonal cycle over Los Angeles, where the filling of the MOZAIC unvisited tropospheric remainder has modified the seasonal cycle, and (2)

[9] Tropospheric Emission Spectrometer.

[10] Atmospheric InfraRed Sounder.

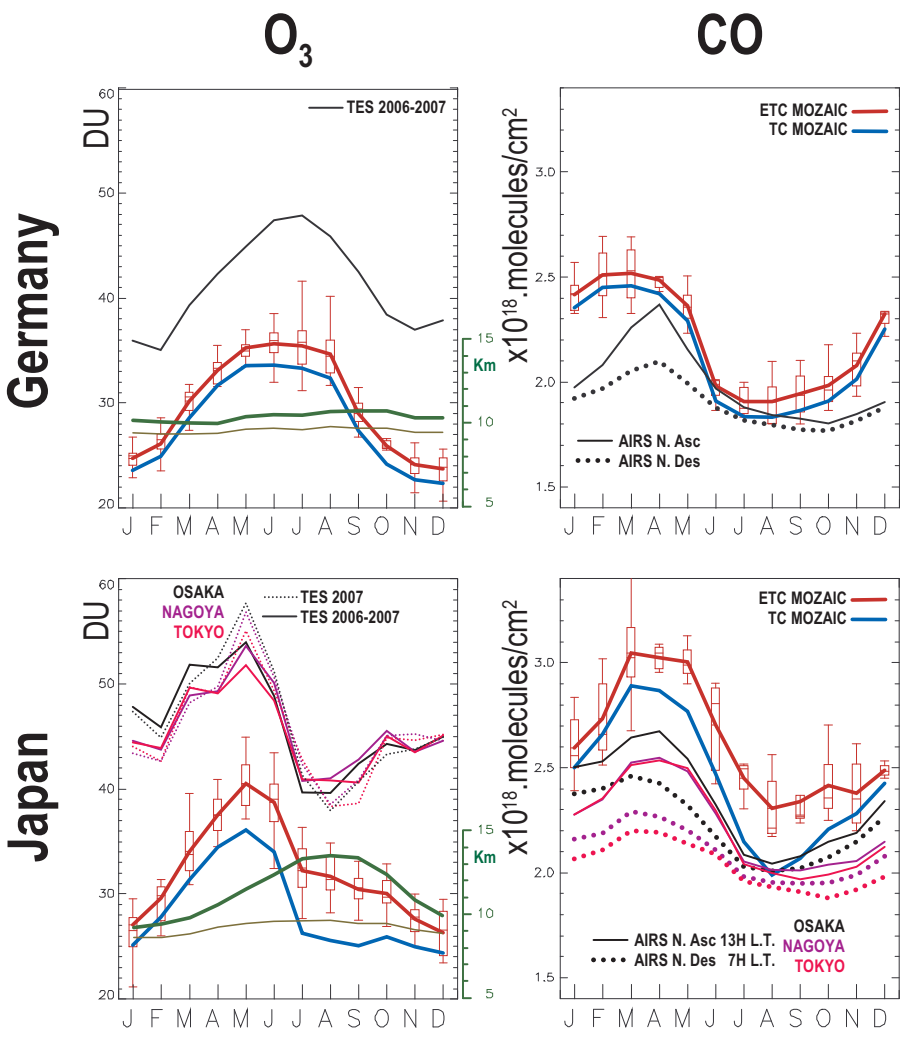

Fig. 13. Seasonal cycles MOZAIC PTC and satellite comparison, i.e. $PTC_m(O_3)$ with TES O_3 tropospheric columns (left, in DU) and $PTC_m(CO)$ with AIRS CO total columns (right, in $\times 10^{18}$ molecules cm^{-2}) over Germany (top) and Japan (bottom). MOZAIC TC is the blue line and PTC the red line with box-and-whisker plots (as in Fig. 5). The solid green line, z_{DT}, and the dotted green line, as defined in Fig. 4, (in kilometres, right green vertical axis) show the unvisited tropospheric layer, Δ. The satellite results are plotted in black over Germany, and in pink, black and purple over Japan for Tokyo, Osaka and Nagoya, respectively. AIRS CO results are given twice a day for ascending node (13:00 LT, solid line) and descending node (07:00 LT, dotted line). O_3 tropospheric columns from TES in 10^{18} molecules cm^{-2} over the periods 2006–2007 or 2007 (solid lines or dotted lines) are converted into DU dividing by 2.686×10^{16}.

the largest MOZAIC tropospheric O_3 column in summer ($>$ 40–45 DU) over Eastmed. Nevertheless, the OMI/MLS summer results over Japan (Ziemke et al., 2011, Fig. 5b) show a June maximum and remains high in July–August, whereas MOZAIC starts a sharp decline.

Although OMI gives global distributions of tropospheric ozone, TES is the first spaceborne instrument to provide vertically resolved information on tropospheric O_3, despite a low sensitivity below 900 hPa (Osterman et al., 2008). For these reasons, we now consider the seasonal cycles of the pure tropospheric O_3 derived from MOZAIC and the tropospheric results from TES (Fig. 13, left). Over Germany, the correlation is excellent ($r = 0.93$), with a TES positive bias of 9–14 DU. The O_3 seasonal cycles (Fig. 13, top left) are well phased with a summer maximum and a winter minimum. Interestingly, a larger winter TES positive bias, by 2–3 DU, is visible. Over Japan, a strong May maximum is observed on both cycles, and an additional secondary winter maximum is detected by TES (Fig. 13, bottom left). Consequently, the correlation drops to $r = 0.60$–0.76, with a TES positive bias of 9–18 DU. These results are consistent with, but all higher than, the 7 DU (2.8 DU) bias found by comparing TES tropospheric columns (with the averaging kernel applied) with 1425 sondes, as reported by Osterman et al. (2008). Herman and Osterman (2011) have reported that the "TES ozone profiles are positively biased (by less than 15 %)

from the surface to the upper troposphere (from ∼ 1000 to 100 hPa) and negatively biased (by less than 20 %) from the upper troposphere to the lower stratosphere (from 100 to 30 hPa) when compared to the ozone-sonde data". Thus, besides the bias due to the instrument vertical resolution and/or the retrieval technique (not discussed here), the differences between MOZAIC and TES are reinforced because, firstly, the observation time influences the O_3 measured in the BL: TES' orbit is sun-synchronous with a 13:43 LT ascending node, comparable to OMI/MLS, while MOZAIC depends on commercial aircraft schedules. The 0–2 km partial column difference in the seasonal cycle using MOZAIC observations over Frankfurt selected at 02:00–06:00 and 11:00–18:00 LT is evaluated to be 2 DU maximum (not shown). Secondly, MOZAIC is almost insensitive to hydrometeorological conditions, while TES data processing requires cloud screening, thus introducing a probable bias due to specific meteorological conditions of sampling. Nonetheless, how can such enlarged winter in situ and spaceborne differences (> 3 DU) be explained at those two sites? In winter, the BL and MT have the lowest O_3 contributions (Fig. 12, top) and z_{DT} is at a minimum. This suggests that the tropopause positioning makes the main contribution to the winter differences, probably because of the 6–7 km vertical resolution of TES measurements and that the tropospheric ozone column might contain some stratospheric information as reported by Osterman et al. (2008). We agree with Stajner et al. (2008), who emphasized the impact of tropopause location on tropospheric O_3 columns, inter-annual variability and trend estimates. Insufficient accuracy in the characterization of the tropopause altitude leads to strong stratospheric contamination in the pure tropospheric O_3 reservoir (Fig. 2) and thus may impact the assessment of trends in the UT.

4.4.2 Carbon monoxide

The AIRS seasonal cycles of total columns and our pure tropospheric seasonal cycles are correlated by $r = 0.89$ ($r = 0.80$) on the descending (ascending) node over Germany. They show a larger difference in winter and a similar response at the summer minimum (Fig. 13, right). As the CO maximum along the vertical is below 2 km and as the impact of tropopause height is negligible, the winter difference may be explained by the weak sensitivity of the satellite instrument in the BL. The winter maximum is clearly not well captured by AIRS. Diurnal variations are zero from July to January and maximum in April. Considering Japan (Fig. 13, bottom right), the correlations are $r = 0.96$–0.98 on the ascending node (13:00 LT) and $r = 0.93$–0.97 on descending node (07:00 LT). From AIRS, we observe differences on the diurnal CO cycle which are larger in winter–spring and almost zero in summer. They also show a west-to-east negative gradient between the individual Japanese airports. In summer, we note that the best agreement is over Germany and that there is excellent agreement between our pure tropospheric seasonal cycles and AIRS in that season (Fig. 13, top right). The differences may be due to less thermal contrast between air in the lower BL and in the surface layer. Besides the low AIRS sensitivity in the BL, an additional source of differences is the cloud screening, a mandatory constraint for AIRS but not required for MOZAIC inducing a sampling effect in the intercomparison.

5 Conclusions

A new and comprehensive O_3 and CO pure tropospheric climatology has been derived from MOZAIC over 1994–2009 including 40 000 profiles. Eleven sites were documented between 24 and 50° N and from Los Angeles to Japan in order to give a quasi-global picture of the northern mid-latitudes. The previous low-biased tropospheric O_3 climatology (Zbinden et al., 2006) has been improved by adding the complete estimate of the MOZAIC unvisited tropospheric remainder as well as CO. The outcome is a fully defined pure tropospheric climatology from the ground to the individual dynamical tropopause based solely on the MOZAIC individual profiles. The O_3 validation was performed using composite results derived from coincident MOZAIC profiles and WOUDC soundings close to the most documented MOZAIC sites (USeast, Germany, Japan). The pure O_3 tropospheric columns reproduce 96–98 % of the composite tropospheric columns after the addition of WOUDC partial columns to MOZAIC when necessary. Therefore, the pure tropospheric profiles (by season) and columns (by month) are the most robust and accurate vertically integrated results based on in situ measurements. As far as we know, this is the first pure tropospheric climatology and is significantly different from climatological profiles at all the sites, as seen in particular for ozone or by referring to Logan (1994), McPeters et al. (2007), Stajner et al. (2008), Ding et al. (2008) and Tilmes et al. (2012).

The first outcome is that the seasonal cycles of the pure tropospheric columns are in the range of 23.7–43.2 DU for O_3 and 1.5–6.8×10^{18} molecules cm^{-2} for CO. Due to the photochemistry and OH removal efficiency, the maxima of the seasonal cycles are not in phase: February–April for CO, May–July for O_3. In terms of zonal variability, for O_3 we globally observe greater summer contents over the northern US, the lowest contents regardless of the months considered over Europe and the greatest spring and summer contents in the Middle East and Beijing. The summer Asian monsoon results in a sharp decrease over Japan, not observed over Beijing, and, surprisingly, in a weakened maximum over Uaemi. In addition, Los Angeles is almost in the range of Asian pollution, except in summer, when incoming air from the Pacific likely strongly interplays. We found that Los Angeles is at the lowest sampling rate acceptable to be included in a climatological study. For CO, the Beijing minimum exceeds the maxima of all other sites for all seasons. The smallest

amplitudes and the lowest winter–spring CO columns are detected in the Middle East.

The second outcome is the seasonal pure tropospheric profile climatology. At all sites, the O_3 pure tropospheric profiles, in DU, never return to a positive vertical gradient above 2 km (except on the poorly sampled winter profiles of Los Angeles), unlike the monthly averaged MOZAIC O_3 profiles. The spring–summer/autumn–winter seasonal dichotomy on O_3 seasonal profiles is confirmed, as is the deep summer decrease due to the monsoon over Japan, Beijing and USsouth with different intensities. Comparing Uaemi with Eastmed in summer, a strong negative O_3 anomaly below 6 km appears. It could be linked to the impact of sea breeze or depleted maritime air inflow from regions under Indian monsoon conditions. Regarding CO, we observe a summer–autumn/winter–spring dichotomy with a clear winter maximum in the BL. Note that in the BL, the CO winter maximum over Beijing is 2–7 times (2–6 times) greater than over Japan (Europe), whereas only 2 times greater above 5 km. Additionally, comparing CO for all the sites in winter at 5 km, the minimum is encountered over the Middle East and southwestern US sites, while north-eastern US sites and Europe show both comparable and higher amounts in contrast to the strong Asian maximum values. The vertical profile study shows a large O_3 and CO homogeneity among the European sites with a west-to-east gradient. We found the upper pure tropospheric layers to be very consistent among chemical species, namely with less O_3 and more CO than when tropospheric/stratospheric reservoirs were undifferentiated, even if monthly averaged profiles were limited to the monthly averaged tropopause altitude.

For the third outcome, we provide the seasonal cycles of the BL, MT and UT partial columns using a new monthly varying criterion, z_{Ld}, as the MT ceiling because of their distinct predominant processes. Consequently, the tropopause of all individual profiles within the time series will always be above z_{Ld}, and thus UT is more faithfully represented. The z_{Ld} is detected at 6–12 km on average, with a winter minimum and summer maximum. This approach highlights a predominant increase (decrease) in the MT O_3 amount associated with a summer- (winter-) wide MT thickening (thinning). The UT O_3 seasonal cycle, maximized earlier than when a fixed ceiling was used, is now more comparable to the UT O_3 seasonal cycle defined using a tropopause reference (Thouret et al., 2006). For CO, it is interesting to note that the clear MT spring maximum is shifted to a broad April–August maximum, in contrast to what happens in the UT.

The last outcome highlights the benefits of this pure tropospheric climatology based on in situ measurements by comparing the seasonal cycles of the MOZAIC tropospheric columns with those derived from satellites. We focused on two sites, Germany and Japan, because of their contrasting tropopause altitude and seasonal variability. We found consistent seasonal cycles from MOZAIC and satellite data, although with noteworthy differences: (1) for O_3, TES tropospheric columns are correlated with MOZAIC by $r = 0.6$ (Japan) and $r = 0.9$ (Germany) and are greater than MOZAIC by 9–18 DU, and the largest biases occur in winter; (2) for CO, AIRS total columns provide a response as much as 1.0×10^{18} molecules cm^{-2} lower than MOZAIC ($r > 0.9$). Besides the instrumental bias, the tropopause is a probable source of discrepancy because just below the monthly tropopause, the MOZAIC profile $MP_m(O_3)$ exceeds our fully defined and pure tropospheric profile. We noted a greater O_3 bias in winter, when the tropopause is low (2–3 DU over Germany, > 5 DU over Japan). Therefore, the O_3 difference is probably mostly explained by stratospheric air contamination but is also explained by clear-sky conditions or the satellite overpass time capturing the daily maximum. All three factors can enhance the satellite response. We point out the need for accurate discrimination between the stratospheric and tropospheric reservoirs, and indeed the monthly tropopause is an unappropriated criterion. This point is crucial, merits consideration and must be clarified within the framework of tropospheric trends and radiative transfer studies.

These fully defined and pure tropospheric products will be available in the MOZAIC/IAGOS database to the scientific community. Such climatologies will be regularly updated thanks to the ongoing MOZAIC programme, IAGOS, whose database is available at http://www.iagos.org/.

Acknowledgements. The authors gratefully acknowledge F. Karcher, who is deeply involved in the MOZAIC/IAGOS programme. Acknowledgements are addressed to the European Commission for their strong support as well as to Airbus and the airlines (Lufthansa, Austrian, Air France) who have carried the MOZAIC equipment and performed its maintenance free of charge since 1994. MOZAIC is presently funded by INSU-CNRS (France), Météo-France, and Forschungszentrum Jülich (FZJ, Jülich, Germany), and the database is supported by ETHER (CNES and INSU-CNRS). We also thank the German Weather Service (Meteorological Observatory at Hohenpeissenberg), the National Space Development Agency of Japan and NASA (Wallops Island Flight Facility) for providing their data through the World Ozone and Ultraviolet Radiation Data Centre (WOUDC) operated by Environment Canada, Toronto, Ontario, Canada, under the auspices of the World Meteorological Organization. The remote sensing data were acquired as part of NASA's Earth-Sun System Division and archived and distributed by the Goddard Earth Sciences (GES) Data and Information Services Center (DISC) Distributed Active Archive Center (DAAC). We acknowledge the mission scientists and principal investigators who provided the TES and AIRS data used in this research through the Giovanni website (http://disc.sci.gsfc.nasa.gov/giovanni/).

Edited by: A. Pozzer

The publication of this article is financed by CNRS-INSU.

References

Aghedo, A. M., Bowman, K. W., Worden, H. M., Kulawik, S. S., Shindell, D. T., Lamarque, J. F., Faluvegi, G., Parrington, M., Jones, D. B. A., and Rast, S.: The vertical distribution of ozone instantaneous radiative forcing from satellite and chemistry climate models, J. Geophys. Res., 116, D01305, doi:10.1029/2010JD014243, 2011.

Agusti-Panareda, A., Gray, S. L., and Methven, J.: Numerical modelling study of boundary-layer ventilation by a cold front over Europe, J. Geophys. Res., 110, D18304, doi:10.1029/2004JD005555, 2005.

Auvray, M. and Bey, I.: Long-range transport to Europe: seasonal variations and implications for the European ozone budget, J. Geophys. Res., 110, D11303, doi:10.1029/2004JD005503, 2005.

Bak, J., Liu, X., Wei, J. C., Pan, L. L., Chance, K., and Kim, J. H.: Improvement of OMI ozone profile retrievals in the upper troposphere and lower stratosphere by the use of a tropopause-based ozone profile climatology, Atmos. Meas. Tech., 6, 2239–2254, doi:10.5194/amt-6-2239-2013, 2013.

Baumannn, K., Maurer, H., Rau, G., Piringer, M., Pechinger, U., Prévôt A., Furgerb, M., Neiningerc, B., and Pellegrini, U.: The influence of south Foehn on the ozone distribution in the Alpine Rhine valley – results from the MAP field phase, Atmos. Environ., 35, 6379–6390, doi:10.1016/S1352-2310(01)00364-8, 2001.

Beer, R., Glavich, T. A., and Rider, D. M.: Tropospheric emission spectrometer for the Earth Observing System's Aura Satellite, Appl. Optics, 40, 2356–2367, 2001.

Brown-Steiner, B. and Hess, P.: Asian influence on surface ozone in the United States: a comparison of chemistry, seasonality, and transport mechanisms, J. Geophys. Res., 116, D17309, doi:10.1029/2011JD015846, 2011.

Clerbaux, C., George, M., Turquety, S., Walker, K. A., Barret, B., Bernath, P., Boone, C., Borsdorff, T., Cammas, J. P., Catoire, V., Coffey, M., Coheur, P.-F., Deeter, M., De Mazière, M., Drummond, J., Duchatelet, P., Dupuy, E., de Zafra, R., Eddounia, F., Edwards, D. P., Emmons, L., Funke, B., Gille, J., Griffith, D. W. T., Hannigan, J., Hase, F., Höpfner, M., Jones, N., Kagawa, A., Kasai, Y., Kramer, I., Le Flochmoën, E., Livesey, N. J., López-Puertas, M., Luo, M., Mahieu, E., Murtagh, D., Nédélec, P., Pazmino, A., Pumphrey, H., Ricaud, P., Rinsland, C. P., Robert, C., Schneider, M., Senten, C., Stiller, G., Strandberg, A., Strong, K., Sussmann, R., Thouret, V., Urban, J., and Wiacek, A.: CO measurements from the ACE-FTS satellite instrument: data analysis and validation using ground-based, airborne and spaceborne observations, Atmos. Chem. Phys., 8, 2569–2594, doi:10.5194/acp-8-2569-2008, 2008.

Cooper, O. R., Stohl, A., Eckhardt, S., Parrish, D. D., Oltmans, S. J., Johnson, B. J., Nédélec P., Schmidlin, F. J., Newchurch, M. J., Kondo, Y., and Kita, K.: A springtime comparison of tropospheric ozone and transport pathways on the east and west coasts of the United States, J. Geophys. Res., 110, D05S90, doi:10.1029/2004JD005183, 2005.

Cooper, O. R., Stohl, A., Trainer, M., Thompson, A. M., Witte, J. C., Oltmans, S. J., Morris, G., Pickering, K. E., Crawford, J. H., Chen, G., Cohen, R. C., Bertram, T. H., Wooldridge, P., Perring, A., Brune, W. H., Merrill, J., Moody, J. L., Tarasick, D., Nédélec P., Forbes, G., Newchurch, M. J., Schmidlin, F. J., Johnson, B. J., Turquety, S., Baughcum, S. L., Ren, X., Fehsenfeld, F. C., Meagher, J. F., Spichtinger, N., Brown, C. C., McKeen, S. A., McDermid, I. S., and Leblanc, T.: Large upper tropospheric ozone enhancements above midlatitude North America during summer: in situ evidence from the IONS and MOZAIC ozone measurement network, J. Geophys. Res., 111, D24S05, doi:10.1029/2006JD007306, 2006.

Cooper, O. R., Parrish, D. D., Stohl, A., Trainer, M., Nédélec P., Thouret, V., Cammas, J. P., Oltmans, S. J., Johnson, B. J., Tarasick, D., Leblanc, T., McDermid, I. S., Jaffe, D., Gao, R., Stith, J., Ryerson, T., Aikin, K., Campos, T., Weinheimer, A., and Avery, M. A.: Increasing springtime ozone mixing ratios in the free troposphere over western North America, Nature, 463, 344–348, doi:10.1038/nature08708, 2010.

Danielsen, E. F.: Stratospheric-tropospheric exchange based on radioactivity, ozone and potential vorticity, J. Atmos. Sci., 25, 502–528, 1968.

de Laat, A. T. J., Gloudemans, A. M. S., Aben, I., Meirink, J. F., Krol, M., van der Werf, G., and Schrijver, H., SCIAMACHY carbon monoxide total columns: Statistical evaluation and comparison with CTM results, J. Geophys. Res., 112, D12310, doi:10.1029/2006JD008256, 2007.

Deeter, M. N., S. Martínez-Alonso, D. P. Edwards, L. K. Emmons, J. C. Gille, H. M. Worden, J. V. Pittman, B. C. Daube, and S. C. Wofsy, Validation of MOPITT Version 5 thermal-infrared, near-infrared, and multispectral carbon monoxide profile retrievals for 2000–2011, J. Geophys. Res. Atmos., 118, 6710–6725, doi:10.1002/jgrd.50272, 2013.

Ding, A. J., Wang, T., Thouret, V., Cammas, J.-P., and Nédélec, P.: Tropospheric ozone climatology over Beijing: analysis of aircraft data from the MOZAIC program, Atmos. Chem. Phys., 8, 1–13, doi:10.5194/acp-8-1-2008, 2008.

Eager, R. E., Raman, S., Wootten, A., Westphal, D. L., Reid, J. S., and Al Mandoos, A.: A climatological study of the sea and land breezes in the Arabian Gulf region, J. Geophys. Res., 113, D15106, doi:10.1029/2007JD009710, 2008.

Emmons, L. K., Edwards, D. P., Deeter, M. N., Gille, J. C., Campos, T., Nédélec, P., Novelli, P., and Sachse, G.: Measurements of Pollution In The Troposphere (MOPITT) validation through 2006, Atmos. Chem. Phys., 9, 1795–1803, doi:10.5194/acp-9-1795-2009, 2009.

Felzer, B. S., Cronin, T., Reilly, J. M., Melillo, J. M., and Wang, X.: Impacts of ozone on trees and drops, C. R. Geosci., 339, 784–798, doi:10.1016/j.crte.2007.08.008, 2007.

Fishman, J. and Larsen, J. C.: Distribution of tropospheric ozone determined from satellite data, J. Geophys. Res., 95, 3599–3617, 1990.

Forster de P. M., and Shine, K. P.: Radiative forcing and temperature trends from stratospheric ozone changes, J. Geophys. Re., 102, 10841–10855, 1997.

Guttikunda, S. K., Tang, Y., Carmichael, G. R., Kurata, G., Pan, L., Streets, D. G., Woo, J.-H., Thongboonchoo, N., and

Fried, A.: Impacts of Asian megacity emissions on regional air quality during spring 2001, J. Geophys. Res., 110, D20301, doi:10.1029/2004JD004921, 2005.

Hegglin, M. I., Boone, C. D., Manney, G. L., Shepherd, T. G., Walker, K. A., Bernath, P. F., Daffer, W. H., Hoor, P., and Schiller, C.: Validation of ACE-FTS satellite data in the upper troposphere/lower stratosphere (UTLS) using non-coincident measurements, Atmos. Chem. Phys., 8, 1483–1499, doi:10.5194/acp-8-1483-2008, 2008.

Herman, R. and Osterman, G.: Earth Observing System (EOS) Tropospheric Emission Spectrometer (TES) Data Validation Report (Version F05_05, F05_06, F05_07 data), Jet Propulsion Laboratory, California Institute of Technology, Pasadena, California, 99 pp., 23 November 2011.

Hoskins, B. J., McIntyre, M. E., and Robertson, A. W. On the use and significance of isentropic potential vorticity maps, Q. J. Meteorol. Soc., 111, 877–946, 1985.

Jaffe, D. and Ray, J.: Increase in surface ozone at rural sites in the western US, Atmos. Environ., 41, 5452–5463, doi:10.1016/j.atmosenv.2007.02.034, 2007.

Jaffe, D., Price, H., Parrish, D., Goldstein, A., and Harris, J.: Increasing background ozone during spring on the west coast of North America, Geophys. Res. Lett., 30, 1613, doi:10.1029/2003GL017024, 2003.

Junge, C. E.: Global ozone budget and exchange between stratosphere and troposphere, Tellus, 14, 363–377, 1962.

Kaiser, A.: Origin of polluted air masses in the Alps. An overview and first results for MONARPOP, Environ. Pollut., 157, 3232–3237, doi:10.1016/j.envpol.2009.05.042, 2009.

Kar, J., Trepte, C. R., Thomason, L. W., Zawodny, J. M., Cunnold, D. M., and Wang, H. J.: On the tropospheric mequrements of ozone by the Stratospheric Aerosol and Gas Experiment II (Sage II, version 6.1) in the tropics, Geophys. Res. Lett., 29, 2208, doi:10.1029/2002GL016241, 2002.

Kar, J., Drummond, J. R., Jones, D. B. A., Liu, J., Nichitiu, F., Zou, J., Gille, J. C., Edwards, D. P., and Deeter, M. N.: Carbon monoxide (CO) maximum over the Zagros mountains in the Middle East: Signature of mountain venting?, Geophys. Res. Lett., 33, L15819, doi:10.1029/2006GL026231, 2006.

Lamsal L. N., Martin R. V., Donkelaar A. van, Celarier E. A., Bucsela E. J., Boersma K. F., Dirksen R., Luo C., and Wang Y., Indirect validation of tropospheric nitrogen dioxide retrieved from the OMI satellite instrument: Insight into the seasonal variation of nitrogen oxides at northern midlatitudes, J. Geophys. Res., 115, D05302, doi:10.1029/2009JD013351, 2010.

Lamsal, L. N., Martin, R. V., Padmanabhan, A., van Donkelaar, A., Zhang, Q., Sioris, C. E., Chance, K., Kurosu, T. P., and Newchurch, M. J.: Application of satellite observations for timely updates to global anthropogenic NO_x emission inventories, Geophys. Res. Lett., 38, L05810, doi:10.1029/2010GL046476, 2011.

Lawrence, M. G. and Lelieveld, J.: Atmospheric pollutant outflow from southern Asia: a review, Atmos. Chem. Phys., 10, 11017—11096, doi:10.5194/acp-10-11017-2010, 2010.

Lelieveld, J., Hoor, P., Jöckel, P., Pozzer, A., Hadjinicolaou, P., Cammas, J.-P., and Beirle, S.: Severe ozone air pollution in the Persian Gulf region, Atmos. Chem. Phys., 9, 1393–1406, doi:10.5194/acp-9-1393-2009, 2009.

Li, Q., Jacob, D. J., Logan, J. A., Bey, I., Yantosca, R. M., Liu, H., Martin, R. V., Fiore, A. M., Field, B. D., and Duncan, B. N.: A tropospheric ozone maximum over the Middle East, Geophys. Res. Lett., 28, 3235–3238, 2001.

Li, Q., Jacob, D. J., Park, R., Wang, Y., Heald, C. L., Hudman, R., Yantosca, R. M., Martin, R. V., and Evans, M.: North American pollution outflow and the trapping of convectively lifted pollution by upper-level anticyclone, J. Geophys. Res., 110, D10301, doi:10.1029/2004JD005039, 2005.

Liu, J., Drummond, J. R., Jones, D. B. A., Cao, Z., Bremer, H., Kar, J., Zou, J., Nichitiu, F., and Gille, J. C.: Large horizontal gradients in atmospheric CO at the synoptic scale as seen by spaceborne Measurements of Pollution in the Troposphere, J. Geophys. Res., 111, D02306, doi:10.1029/2005JD006076, 2006.

Liu, J., Jones, D. B. A., Zhang, S., and Kar, J.: Influence of interannual variations in transport on summertime abundances of ozone over the Middle East, J. Geophys. Res., 116, D20310, doi:10.1029/2011JD016188, 2011.

Logan, J.: Tropospheric ozone seasonal behavior, trends, and anthropogenic influence, J. Geophys. Res., 90, 10463–10482, 1985.

Logan, J.: Trends in the vertical distribution of ozone: an analysis of ozonesonde data, J. Geophys. Res., 94, 25553–25585, 1994.

Logan, J.: An analysis of ozonesonde data for the troposphere: recommendations for testing 3-D models and development of a gridded climatology for tropospheric ozone, J. Geophys. Res., 104, 16115–16149, 1999.

Marenco, A., Thouret, V., Nédélec P., Smit, H., Helten, M., Kley, D., Karcher, F., Simon, P., Law, K., Pyle, J., Poschmann, G., Von Wrede, R., Hume, C., Cook, T.: Measurement of ozone and water vapor by Airbus in-service aircraft: the MOZAIC airborne program, an overview, J. Geophys. Res., 103, 631–642, 1998.

McMillan W. W., Evans K. D., Barnet C. D., Maddy E., Sachse G. W., and Disken G. S.: Validating the AIRS Version 5 CO retrieval with DACOM in situ measurements during INTEX-A and –B, IEEE T. Geosci. Remote, 49, 2802–2813, doi:10.1109/TGRS.2011.2106505, 2011.

McPeters, R. D., Labow, G. J., and Logan, J. A.: Ozone climatological profiles for satellite retrieval algorithms, J. Geophys. Res., 112, D05308, doi:10.1029/2005JD006823, 2007.

Morris G. A., Hersey S., Thompson A. M., Pawson S., Nielsen J. E., Colarco P. R., Wallace McMillan W., Stohl A., Turquety S., Warner J., Johnson B. J., Kucsera T. L., Larko D. E., Oltmans S. J., and Witte J. C., Alaskan and Canadian forest fires exacerbate ozone pollution over Houston, Texas, on 19 and 20 July 2004. J. Geophys. Res., 111, D24S03, doi:10.1029/2006JD007090, 2006.

Nedelec, P., Cammas, J.-P., Thouret, V., Athier, G., Cousin, J.-M., Legrand, C., Abonnel, C., Lecoeur, F., Cayez, G., and Marizy, C.: An improved infrared carbon monoxide analyser for routine measurements aboard commercial Airbus aircraft: technical validation and first scientific results of the MOZAIC III programme, Atmos. Chem. Phys., 3, 1551–1564, doi:10.5194/acp-3-1551-2003, 2003.

Neuman, J. A., Trainer, M., Aikin, K. C., Angevine, W. M., Brioude, J., Brown, S. S., de Gouw, J. A., Dube, W. P., Flynn, J. H., Graus, M., Holloway, J. S., Lefer, B. L., Nedelec, P., Nowak, J. B., Parrish, D. D., Pollack, I. B., Roberts, J. M., Ryerson, T. B., Smit, H., Thouret, V., and Wagner, N. L.: Observations of ozone transport from the free troposphere

to the Los Angeles basin, J. Geophys. Res., 117, D00V09, doi:10.1029/2011JD016919, 2012.

Oltmans, S. J., Lefohn, A. S., Harris, J. M., and Shadwick, D. S.: Background ozone levels of air entering the west coast of the US and assessment of longer-term changes, Atmos. Environ., 42, 6020–6038, 2008.

Osterman, G. B., Kulawik, S. S., Worden, H. M., Richards, N. A. D., Fisher, B. M., Eldering, A., Shephard, M. W., Froidevaux, L., Labow, G., Luo, M., Herman, R. L., Bowman, K. W., and Thompson, A. M.: Validation of Tropospheric Emission Spectrometer (TES) measurements of the total, stratospheric, and tropospheric column abundance of ozone, J. Geophys. Res., 113, D15S16, doi:10.1029/2007JD008801, 2008.

Parrish, D., Dunlea, E. J., Atlas, E. L., Schauffler, S., Donnelly, S., Stroud, V., Goldstein, A. H., Millet, D. B., McKay, M., Jaffe, D. A., Price, H. U., Hess, P. G., Flocke, F., and Roberts, J. M.: Changes in the photochemical environment of the temperate North Pacific troposphere in response to increased Asian emissions, J. Geophys. Res., 109, D23S18, doi:10.1029/2004JD004978, 2004.

Riese, M., Ploeger, F., Rap, A., Vogel, B., Konopka, P., Dameris, M., and Forster, P.: Impact of uncertainties in atmospheric mixing on simulated UTLS composition and related radiative effects, J. Geophys. Res., 117, D16305, doi:10.1029/2012JD017751, 2012.

Schneider, P. and van der A, R. J.: A global single-sensor analysis of 2002–2011 tropospheric nitrogen dioxide trends observed from space J. Geophys. Res., 117, D16309, doi:10.1029/2012JD017571, 2012.

Smit, H. G. J. and Team ASOPOS: Quality assurance and quality control for ozonesonde measurements in GAW, WMO/GAW Rep 201, 2013.

Stajner, I., Wargan, K., Pawson, S., Hayashi, H., Chang, L.-P., Hudman R. C., Froidevaux, L., Livesey, N., Levelt, P. F., Thompson, A. M., Tarasick, D. W., Stübi R., Andersen, S. B., Yela, M., König-Langlo, G., Schmidlin, F. J., and Witte, J. C.: Assimilated ozone from EOS-Aura: evaluation of the tropopause region and tropospheric columns, J. Geophys. Res., 113, D16S32, doi:10.1029/2007JD008863, 2008.

Stohl, A., Bonasoni, P., Cristofanelli, P., Collins, W., Feichter, J., Frank, A., Forster, C., Gerasopoulos, E., Gäggeler H., James, P., Kentarchos, T., Kromp-Kolb, H., Krüger B., Land, C., Meloen, J., Papayannis, A., Priller, A., Seibert, P., Sprenger, M., Roelofs, G. J., Scheel, H. E., Schnabel, C., Siegmund, P., Tobler, L., T. Trickl, T., Wernli, H.,Wirth, V., Zanis, P., and Zerefos, C.: Stratosphere-troposphere exchange: a review and what we have learned from STACCATO, J. Geophys. Res., 108, 8516, doi:10.1029/2002JD002490, 2003.

Susskind, J., Barnet, C. D., and Blaisdell, J. M.: Retrieval of atmospheric and surface parameters from AIRS/AMSU/HSB Data in the presence of clouds, IEEE T. Geosci. Remote, 41, 390–409, doi:10.1109/TGRS.2002.808236, 2003.

Susskind, J., Blaisdell, J., and Rosenkranz, P.: AIRS/AMSU/HSB Version 5 Level 2 Quality Control and Error Estimation Ed: E. T. Olsen Version 1.1 Jet Propulsion Laboratory, California Institute of Technology, Pasadena, CA, USA, 15 pp., March 2010.

Tangborn, A., Stajner, I., Buchwitz, M., Khlystova, I., Pawson, S., Burrows, J., Hudman, R., and Nédélec P.: Assimilation of SCIAMACHY total column CO observations: global and regional analysis of data impact, J. Geophys. Res., 114, D07307, doi:10.1029/2008JD010781, 2009.

Thouret, V., Marenco, A., Logan, J. A., Nédélec P., and Grouhel, C.: Comparisons of ozone measurements from the MOZAIC airborne program and the ozone sounding network at eight locations, J. Geophys. Res., 103, 695–720, 1998.

Thouret, V., Cammas, J.-P., Sauvage, B., Athier, G., Zbinden, R., Nédélec, P., Simon, P., and Karcher, F.: Tropopause referenced ozone climatology and inter-annual variability (1994–2003) from the MOZAIC programme, Atmos. Chem. Phys., 6, 1033–1051, doi:10.5194/acp-6-1033-2006, 2006.

Tilmes, S., Lamarque, J.-F., Emmons, L. K., Conley, A., Schultz, M. G., Saunois, M., Thouret, V., Thompson, A. M., Oltmans, S. J., Johnson, B., and Tarasick, D.: Technical Note: Ozonesonde climatology between 1995 and 2011: description, evaluation and applications, Atmos. Chem. Phys., 12, 7475–7497, doi:10.5194/acp-12-7475-2012, 2012.

Turquety, S., Logan, J. A., Jacob, D. J., Hudman, R. C., Leung, F. Y., Heald, C. L., Yantosca, R. M., Wu, S., Emmons, L. K., Edwards, D. P., and Sachse, G. W.: Inventory of boreal fire emissions for North America in 2004: Importance of peat burning and pyroconvective injection, J. Geophys. Res., 112, D12S03, doi:10.1029/2006JD007281, 2007.

van der A, R. J., Eskes, H. J., Boersma, K. F., van Noije, T. P. C., Van Roozendael, M., De Smedt, I., Peters, D. H. M. U., and Meijer, E. W.: Trends, seasonal variability and dominant NO_x source derived from a ten year record of NO_2 measured from space, J. Geophys. Res., 113, D04302, doi:10.1029/2007JD009021, 2008.

Voulgarakis, A., Telford, P. J., Aghedo, A. M., Braesicke, P., Faluvegi, G., Abraham, N. L., Bowman, K. W., Pyle, J. A., and Shindell, D. T.: Global multi-year O_3-CO correlation patterns from models and TES satellite observations, Atmos. Chem. Phys., 11, 5819–5838, doi:10.5194/acp-11-5819-2011, 2011.

Wang, Y., Konopka, P., Liu, Y., Chen, H., Müller, R., Plöger, F., Riese, M., Cai, Z., and Lü, D.: Tropospheric ozone trend over Beijing from 2002–2010: ozonesonde measurements and modeling analysis, Atmos. Chem. Phys., 12, 8389–8399, doi:10.5194/acp-12-8389-2012, 2012.

Warneke C., de Gouw J. A., Del Negro L., Brioude J., McKeen S., Stark H., Kuster W. C., Goldan P. D., Trainer M., Fehsenfeld F. C., Wiedinmyer C., Guenther A. B., Hansel A., Wisthaler A., Atlas E., Holloway J. S., B. Ryerson T., Peischl J., Huey L. G., and Case Hanks A. T.: Biogenic emission measurement and inventories determination of biogenic emissions in the eastern United States and Texas and comparison with biogenic emission inventories, J. Geophys. Res., 115, D00F18, doi:10.1029/2009JD012445, 2010.

Wernli, H. and Bourqui, M.: A Lagrangian "one-year climatology" of (deep) cross-tropopause exchange in the extratropical Northern Hemisphere, J. Geophys. Res., 107, 4021, doi:10.1029/2001JD000812, 2002.

West, J. J., Szopa, S., and Hauglustaine, D. A.: Human mortality effects of future concentrations of tropospheric ozone, C. R. Geosci., 339, 775–783, doi:10.1016/j.crte.2007.08.005, 2007.

World Meteorological Organisation (WMO): Meteorology – A three dimensional science, WMO Bulletin, 6, 134–138, 1957.

Worden, H. M., Logan, J. A., Worden, J. R., Beer, R., Bowman, K., Clough, S. A., Eldering, A., Fisher, B. M., Gunson, M. R., Herman, R. L., Kulawik, S. S., Lampel, M. C., Luo, M., Megret-

skaia, I. A., Osterman, G. B., and Shephard, M. W.: Comparisons of Tropospheric Emission Spectrometer (TES) ozone profiles to ozonesondes: methods and initial results, J. Geophys. Res.-Atmos., 112, D03309, doi:10.1029/2006JD007258, 2007.

Yurganov, L. N., Blumenstock, T., Grechko, E. I., Hase, F., Hyer, E. J., Kasischke, E. S., Koike, M., Kondo, Y., Kramer, I., Leung, F.-Y., Mahieu, E., Mellqvist, J., Notholt, J., Novelli, P. C., Rinsland, C. P., Scheel, H. E., Schulz, A., Strandberg, A., Sussmann, R., Tanimoto, H., Velazco, V., Zander, R., and Zhao, Y.: A quantitative assessment of the 1998 carbon monoxide emission anomaly in the Northern Hemisphere based on total column and surface concentration measurements, J. Geophys. Res., 109, D15305, doi:10.1029/2004JD004559, 2004.

Zbinden, R. M., Cammas, J.-P., Thouret, V., Nédélec, P., Karcher, F., and Simon, P.: Mid-latitude tropospheric ozone columns from the MOZAIC program: climatology and interannual variability, Atmos. Chem. Phys., 6, 1053-1073, doi:10.5194/acp-6-1053-2006, 2006.

Zhang, L., Jacob, D. J., Bowman, K. W., Logan, J. A., Turquety, S., Hudman, R. C., Li, Q., Beer, R., Worden, H. M., Worden, J. R., Rinsland, C. P., Kulawik, S. S., Lampel, M. C.,Shephard M. W., Fisher, B. M., Eldering, A., and Avery,M. A.: Ozone-CO correlations determined by the TES satellite instrument in continental outflow regions, Geophys. Res. Lett., 33, L18804, doi::10.1029/2006GL026399, 2006

Ziemke, J. R., Chandra, S., Labow, G. J., Bhartia, P. K., Froidevaux, L., and Witte, J. C.: A global climatology of tropospheric and stratospheric ozone derived from Aura OMI and MLS measurements, Atmos. Chem. Phys., 11, 9237–9251, doi:10.5194/acp-11-9237-2011, 2011.